NASA/TP–2012-217584

Design, Optimization, and Evaluation of A1-2139 Compression Panel with Integral *T*-Stiffeners

Sameer B. Mulani
Virginia Polytechnic Institute and State University, Blacksburg, Virginia

David Havens
Lockheed Martin Aeronautics Company, Marietta, Georgia

Ashley Norris
Lockheed Martin Aeronautics Company, Palmdale, California

R. Keith Bird
Langley Research Center, Hampton, Virginia

Rakesh K. Kapania
Virginia Polytechnic Institute and State University, Blacksburg, Virginia

Robert Olliffe
Lockheed Martin Aeronautics Company, Marietta, Georgia

June 2012

NASA STI Program . . . in Profile

Since its founding, NASA has been dedicated to the advancement of aeronautics and space science. The NASA scientific and technical information (STI) program plays a key part in helping NASA maintain this important role.

The NASA STI program operates under the auspices of the Agency Chief Information Officer. It collects, organizes, provides for archiving, and disseminates NASA's STI. The NASA STI program provides access to the NASA Aeronautics and Space Database and its public interface, the NASA Technical Report Server, thus providing one of the largest collections of aeronautical and space science STI in the world. Results are published in both non-NASA channels and by NASA in the NASA STI Report Series, which includes the following report types:

- TECHNICAL PUBLICATION. Reports of completed research or a major significant phase of research that present the results of NASA Programs and include extensive data or theoretical analysis. Includes compilations of significant scientific and technical data and information deemed to be of continuing reference value. NASA counterpart of peer-reviewed formal professional papers, but having less stringent limitations on manuscript length and extent of graphic presentations.

- TECHNICAL MEMORANDUM. Scientific and technical findings that are preliminary or of specialized interest, e.g., quick release reports, working papers, and bibliographies that contain minimal annotation. Does not contain extensive analysis.

- CONTRACTOR REPORT. Scientific and technical findings by NASA-sponsored contractors and grantees.

- CONFERENCE PUBLICATION. Collected papers from scientific and technical conferences, symposia, seminars, or other meetings sponsored or co-sponsored by NASA.

- SPECIAL PUBLICATION. Scientific, technical, or historical information from NASA programs, projects, and missions, often concerned with subjects having substantial public interest.

- TECHNICAL TRANSLATION. English-language translations of foreign scientific and technical material pertinent to NASA's mission.

Specialized services also include organizing and publishing research results, distributing specialized research announcements and feeds, providing information desk and personal search support, and enabling data exchange services.

For more information about the NASA STI program, see the following:

- Access the NASA STI program home page at *http://www.sti.nasa.gov*

- E-mail your question to help@sti.nasa.gov

- Fax your question to the NASA STI Information Desk at 443-757-5803

- Phone the NASA STI Information Desk at 443-757-5802

- Write to:
  STI Information Desk
  NASA Center for AeroSpace Information
  7115 Standard Drive
  Hanover, MD 21076-1320

NASA/TP–2012-217584

Design, Optimization, and Evaluation of A1-2139 Compression Panel with Integral *T*-Stiffeners

Sameer B. Mulani
Virginia Polytechnic Institute and State University, Blacksburg, Virginia

David Havens
Lockheed Martin Aeronautics Company, Marietta, Georgia

Ashley Norris
Lockheed Martin Aeronautics Company, Palmdale, California

R. Keith Bird
Langley Research Center, Hampton, Virginia

Rakesh K. Kapania
Virginia Polytechnic Institute and State University, Blacksburg, Virginia

Robert Olliffe
Lockheed Martin Aeronautics Company, Marietta, Georgia

National Aeronautics and
Space Administration

Langley Research Center
Hampton, Virginia 23681-2199

June 2012

Acknowledgments

The work presented here was funded under NASA Subsonic Fixed Wing Hybrid Body Technologies NRA (NASA NNL08AA02C) with Ms. Karen M. Brown Taminger as the NASA Technical Lead. The authors are thankful to Ms. Taminger for her suggestions. The authors would like to thank our partners in the NRA project, Mr. John Barnes and Dr. Steve Englestad of Lockheed Martin Aeronautics Company of Marietta, GA, for technical discussions.

Compression tests were conducted at NASA Langley Research Center under the Subsonic Fixed Wing Program. Ms. Dawn Jegley of the Structural Mechanics and Concepts Branch provided invaluable advice for conducting this compression test.

Available from:

NASA Center for AeroSpace Information
7115 Standard Drive
Hanover, MD 21076-1320
443-757-5802

Abstract

A *T*-stiffened panel was designed and optimized for minimum mass subjected to constraints on buckling load, yielding, and crippling or local stiffener failure using a new analysis and design tool named *EBF3PanelOpt*. The panel was designed for a compression loading configuration, a realistic load case for a typical aircraft skin-stiffened panel. The panel was integrally machined from 2139 aluminum alloy plate and was tested in compression. The panel was loaded beyond buckling and strains and out-of-plane displacements were extracted from 36 strain gages and one linear variable displacement transducer. A digital photogrammetic system was used to obtain full field displacements and strains on the smooth (unstiffened) side of the panel. The experimental data were compared with the strains and out-of-plane deflections from a high-fidelity nonlinear finite element analysis. The test data indicated that the panel buckled at the linear elastic buckling eigenvalue predicted for the panel. The out-of-plane displacement measured by the digital photogrammetic system compared well both qualitatively and quantitatively with the nonlinear finite element solution in the post-buckling regime. Furthermore, the experimental strains compared well with both the linear and nonlinear finite element model prior to buckling. The weight of the optimized panel was 20 percent less than that of a *T*-stiffened panel optimized using conventional design techniques.

THIS PAGE INTENTIONALLY LEFT BLANK

TABLE OF CONTENTS

LIST OF TABLES

LIST OF FIGURES

Nomenclature

3D	three-dimensional
BDF	bulk data format
CAD	computer aided design
CFD	computational fluid dynamics
EBF^3	electronic beam free-form fabrication
FEA	finite element analysis
FEM	finite element model
FSW	friction stir welding
GA	genetic algorithm
LaRC	Langley Research Center
LVDT	linear variable displacement transducer
NASA	National Aeronautics and Space Administration
NC	numerically controlled
NRA	NASA research announcement
NSGA-II	non-dominated sorting algorithm
PSO	particle swarm optimization
a_1	a multiplication constant for allowable crippling stress calculation
a_2	an exponent for allowable crippling stress calculation
b_n	length of n^{th} component of the stiffener cross section, inch
E	Young's modulus, psi
F_{cc}	allowable crippling stress for whole stiffener, psi
F_{cc_n}	allowable crippling stress of n^{th} component of the stiffener cross-section, psi
h_w	height of the web, inch
n	number of components in the stiffener cross section
t_f	flange thickness, inch
t_n	thickness of n^{th} component of the stiffener cross-section, inch
t_p	panel pocket thickness, inch
t_w	web thickness, inch
w_f	flange width, inch
x,y,z	rectilinear coordinate basis
λ_0	buckling eigenvalue
ε	strain
σ_{vm}	von Mises stress, psi
σ_{stiff}	minimum principle stress in the stiffener, psi
σ_y	yield stress, psi
ν	Poisson's ratio

SECTION 1
INTRODUCTION

Stiffened panels are integral parts of aerospace, automobile, and ship structures due to their high stiffness-to-weight ratio as compared to unstiffened panels. These stiffened panels are designed to withstand the buckling, yielding, and crippling of the applied in-plane loads; hence, the optimality of these structures depends upon the appropriate dimensions of the plate and stiffeners and the appropriate stiffener locations. Traditionally, these stiffening members, which have a uniform cross section, are straight and riveted to the panels or to the parent structures to ease the manufacturing process. Over the years optimization frameworks using discrete numbers of straight stiffeners, like Hypersizer (ref. 1), PASCO (ref. 2), PANDA (ref. 3), and VICONOPT (ref. 4) have been developed to optimize stiffened panels. These frameworks rely on the Rayleigh-Ritz method or the finite strip method to do analysis, but they have some limitations when optimizing panels, especially non-rectangular panels, with nonuniform in-plane loading. More information about these limitations can be found in references 4 and 5. Thus, traditional design methodology has a limited design space to achieve a desired performance. A designer can use the enhanced design space by employing curved, nonuniform thickness stiffening members, as well as panel thicknesses, without using riveted joints. This design philosophy uses the concept of *unitized structures*, meaning that the stiffening members become integral to the structures, leading to a monolithic construction of the vehicle and a reduced count of total parts for an assembly (ref. 6).

Mankind's wish for future aerospace vehicles to be multifunctional and have improved performance has led to better vehicles. Additional requirements like fuel efficiency (to combat unstable fuel prices) and reduced emissions have become of prime importance in the last decade. Yet, airlines stipulate that a 20 percent improvement in direct operating cost is necessary to justify introducing an all-new aircraft into their fleets (ref. 6). The aircraft industry is thus forced to continuously reduce the weight of the aircraft. With that goal in mind, National Aeronautics and Space Administration (NASA) has initiated several NASA Research Announcement (NRA) contracts for future aircraft designs that are fuel efficient and have met requirements for reduced emissions and noise. Three different aircraft configurations were included in the NRA as future aerospace vehicles: 1) hybrid wing/body, 2) truss-braced wing, and 3) double bubble. These vehicles would have pressurized noncircular fuselage structures and complex wing geometry. Traditional aircraft designs have led designers to have the confidence and experience of designing such structures using both the knowledge-base that has been built over the years and various other rules-of-thumb. There is a lack of experience in both the knowledge of the structural loads and the resulting design of complex, multi-functional, aircraft structural concepts for future aerospace vehicles.

During the last three decades, there has been tremendous progress in computer-aided design (CAD), the finite element method (FEM), computational fluid dynamics (CFD), and multi-physics modeling using numerical methods. It has led to better analyses of vehicles and reduced the need for extensive experimentation. Because of better analysis tools and the availability of parallel processing, the optimization algorithms have improved substantially. Earlier, gradient-based optimization methods were popular due to their efficiency. Currently, global heuristic optimization techniques, such as genetic algorithm (GA), particle swarm optimization (PSO),

and ant-colony optimization, are increasingly used more because of available computational power and the need for global optimal solutions.

In recent years, topology optimization methods for continuum structures have increased in popularity. Bendsoe and Kikuchi developed the theoretical foundation for the topology optimization methodology in 1988 (ref. 7). The commercial software, Altair OptiStruct (ref. 8), was developed and released in 1994 and used the topology optimization approach. In topology optimization, the density or elastic modulus of each finite element is allowed to vary between lower and upper bounds (ref. 9). Hence, the number of design variables in the topology optimization is equal to or greater than the number of finite elements. Another issue with topology optimization is the creation of the checker board pattern. To remove a checker board pattern generated during the topology optimization, different filtering schemes are used that add further computational cost. So, topology optimization is very computationally-intensive in its current format. Thus, the method can be impractical for everyday design. Furthermore, the manufacturability of the optimal design is not guaranteed.

However, recent new metallic manufacturing processes such as friction stir welding (FSW) (ref. 10) and electron beam freeform fabrication (EBF^3) (ref. 11) allow the design engineer to consider a more broad design space. Moreover, the topology optimization method often results in curved geometries (e.g., the fillet problem in ref. 7). Therefore, considering a design space in which stiffeners can take a curvilinear profile rather than a straight profile may result in a reduction in mass for the same structural design requirements. By using these innovative manufacturing techniques with curvilinear stiffening, the design engineer can build unitized structures with fewer parts, lower weight, less material wastage, and multifunctionality. In addition, these attributes make unitized structures good candidates for manufacturing in space. Additional benefits of unitized structures are found in reference 12. The use of the unitized structure is expected to grow exponentially by the year 2020 (ref. 6). Boeing (ref. 13) developed an integrally stiffened fuselage concept whose analyses and experimental tests demonstrated equal or better performance than conventional designs with regard to weight and structural integrity, while achieving a significant reduction in manufacturing cost.

Since 2007, an analysis and design tool, *EBF3PanelOpt* (ref. 14–17), has been under development for the design and optimization of complex aircraft structural concepts at the Virginia Polytechnic Institute and State University (Virginia Tech). *EBF3PanelOpt* is a tool for optimization of stiffened panel and shell structures in which stiffeners are not limited by traditional manufacturing techniques. Using curved stiffeners broadens the design space without substantially adding to the computational cost of the optimization. *EBF3PanelOpt* is being developed to exploit the emerging additive manufacturing processes that offer the ability to efficiently fabricate complex structural configurations. Initially, *EBF3PanelOpt* was supported with two or four curvilinear blade-stiffeners, but subsequently, it was extended to support multiple load-cases and nonuniform panel thicknesses. For blade-stiffened panels, in-plane loads are always applied through the plate only, not through the stiffeners. For very high in-plane compression loadings, non-blade stiffeners like *T*, *L*, *J* or hat stiffeners are efficient in load resistance. So, in the last phase, *EBF3PanelOpt* was modified to support curvilinear *T* stiffeners and with the stiffeners loaded (ref. 17). The ultimate goal is to enhance aircraft performance and environmental responsibility through reductions in weight, emissions, and cabin noise, and to

integrate functions such as acoustic damping, adaptive active aerodynamic controls, and aeroelastically tailored structures.

The tool development is being conducted under an NRA contract at Virginia Tech with support and aircraft manufacturing expertise provided through a subcontract with Lockheed Martin Aeronautics Company (LM Aero). The work is complementary to the EBF^3 additive manufacturing research activities at NASA LaRC.

This paper describes the final phase of the development of the *EBF3PanelOpt* using curvilinear *T*-stiffeners. To analyze the advantage of *EBF3PanelOpt* , the baseline panel was optimized with mass minimization as an objective and subjected to constraints on the buckling load, yielding, and crippling or on local stiffener failure under compression loading. The optimized panel design was used to fabricate an integrally-machined test panel with aluminum alloy Al−2139. The panel was tested at NASA LaRC under uniaxial compression loading. The test results were compared against a high-fidelity nonlinear finite element analysis (FEA) of the test panel. During the experimentation, the panel buckled at a critical limit load predicted by *EBF3PanelOpt* and nonlinear FEA. The elastic strains calculated by the nonlinear FEA model matched within just a few percent of the measured values. Even the post-buckling analysis matched within 5 percent of the measured values for strains and loads. The biggest achievement was a 20 percent mass reduction for the *T*-stiffened panel design using *EBF3PanelOpt* over a conventionally optimized panel using current industry practice.

SECTION 2
EBF3PANELOPT FRAMEWORK

In the initial stages of the *EBF3PanelOpt* optimization framework, blade-stiffened panels under multiple load cases could be optimized with *EBF3PanelOpt*, but the stiffeners were not directly loaded during the application of in-plane compression. For larger magnitudes of in-plane compression along with the shear forces, the optimal panel requires the stiffener cross section having a larger moment of area away from neutral axis to resist the buckling efficiently. Hence, the optimal panel design would have non-blade stiffeners like *T*, *L*, or a hat cross section for the stiffeners, but note that these cross sections would be optimal if the stiffeners were loaded directly in compression. So, *EBF3PanelOpt* has been updated to support the curvilinear *T*-stiffeners for panel designs along with the options: 1) loads through the stiffeners and plate, and 2) loads through the plate only (ref. 17).

The *EBF3PanelOpt* optimization framework shown in Fig. 1 is an object-oriented script written in Python that interfaces MSC.PATRAN and MSC.NASTRAN to perform FEA on a panel with curvilinear *T*-type stiffeners. It calculates the mass of the panel and constraints on yielding, buckling, and crippling or local failure of the panel. For further information see reference 17 by Mulani, Duggirala and Kapania.

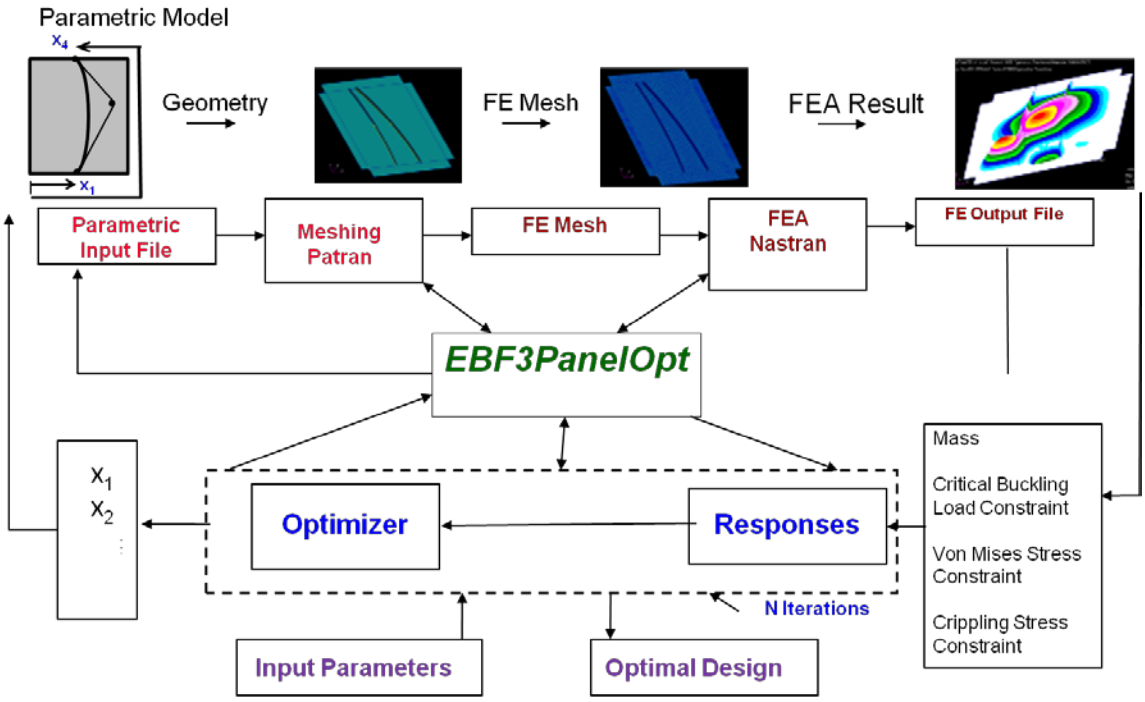

Figure 1. Schematic of *EBF3PanelOpt* framework.

During the optimization, after reading the design variables, Python writes a PATRAN session file, launches PATRAN, and executes this session file to update the geometry of the stiffened panel. After successful execution of the session file, it writes the input file (using the bulk data file or bdf) for NASTRAN. After the successful execution of this NASTRAN (bdf) file, a code written in Python reads the NASTRAN response file (f06) and calculates the responses like the buckling factor, von Mises stress, and crippling stress. These responses are fed to the optimizer to generate new designs or to make a decision regarding the optimization process. During the execution of PATRAN and NASTRAN, if any error occurs or if the run takes more time than the allocated time, these processes will be terminated and default responses will be sent with "pass/fail" as an active constraint. Many other checks are implemented to monitor the successful completion of geometry, meshing whole geometry, and evaluation of finite element analysis.

Here, the optimization goal is to minimize the mass of the panel with the constraints on global buckling, von Mises stress, and crippling or local failure of the stiffeners. The buckling constraint is calculated by:

$$\frac{1}{\lambda_0} \le 1 \tag{1}$$

where λ_0 is the buckling eigenvalue. The von Mises stress constraint is calculated by:

$$\frac{\sigma_{vm}}{\sigma_y} \le 1 \tag{2}$$

where σ_{vm} is the von Mises stress, and σ_y is the material yield strength. The von Mises stress constraint is imposed using the Kreisselmeier-Steinhauser criteria for constraint aggregation as described in reference 18. The crippling constraint was calculated by:

$$\frac{\sigma_{stiff}}{F_{cc}} \le 1 \tag{3}$$

where σ_{stiff} was taken as the minimum principal stress in the stiffener and where F_{cc} is the maximum allowable stress in the stiffener with a complex cross section that is calculated with the weighted formula given by:

$$F_{cc} = \frac{\sum_n b_n t_n F_{cc_n}}{\sum_n b_n t_n} \tag{4}$$

where b_n, t_n, n and F_{ccn} are length, thickness of the stiffener's individual component, total number of components of the stiffener cross section, and maximum allowable crippling stress for an individual component of the stiffener given by:

$$F_{cc} = \begin{cases} \sigma_y, & a_1\left(\dfrac{b\sqrt{\sigma_y / E}}{t}\right)^{-a_2} > 1 \\ a_1\sigma_y\left(\dfrac{b\sqrt{\sigma_y / E}}{t}\right)^{-a_2}, & a_1\left(\dfrac{b\sqrt{\sigma_y / E}}{t}\right)^{-a_2} \le 1 \end{cases} \tag{5}$$

where E is the Young's modulus of the stiffener material, b and t are the length and the thickness of the stiffener cross-section member, respectively. The coefficients a_1 and a_2 are *0.61525* and *0.78387*, respectively, for the stiffener member that is free at one end and connected to another member or structure at the other end. For the stiffener member that is connected at both ends, a_1 and a_2 are *1.1819* and *0.7782*, respectively. The maximum allowable stress formula, Eq. 5, was obtained from page 444 of reference 19.

2.1 Parametric Modeling of the Panel

A key ingredient to *EBF3PanelOpt* is the ability to specify the geometry in a parametric fashion such that the optimizer fully specifies the panel shape and size by a discrete number of design variables. Height of the web, thicknesses of the flange and web, and flange width of uniform *T*-stiffener cross section are sizing design variables apart from the plate pocket thicknesses. In *EBF3PanelOpt*, stiffener curve or profile is defined using third order uniform rational B-spline using two endpoints and a control point. The interpolation of the perimeter of the panel and panel surface yields endpoints and the control point for the stiffener. So, four design variables are required to define the stiffener curve, two for endpoints and two for the control point. As shown in Fig. 2(a), design variables x_1 and x_4 define endpoints of the stiffener, and design variables x_2 and x_3 indicate the control points for the typical stiffener curve. Figure 2(b) shows the typical cross section of the stiffener along with the terminology of its parts.

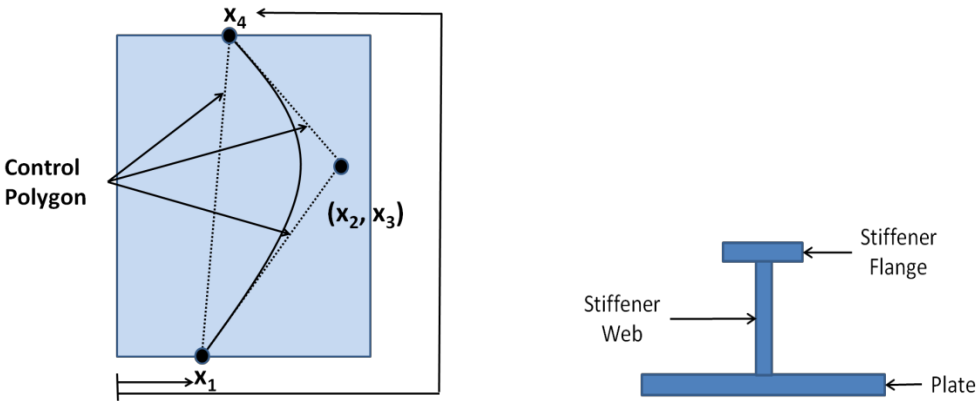

(a) Shape design variables. **(b) *T*-stiffener cross section.**

Figure 2. Design variables for stiffener curve and *T*-stiffener cross-section.

The *EBF3PanelOpt*code has an option for the placement of stiffeners to use the symmetry of the panel. The stiffeners are placed symmetrically with respect to *x* and *y* axes using the ”Symmetric Design” option; only even numbers of stiffeners are used, and the design variables related to only half of the stiffeners are given during the optimization. When the stiffeners are loaded in compression using the option ”Stiffener Loads,” the user has to use the ”Symmetric Design” option. There is another option, called “Nonuniform Thickness,” that provides the different thickness values for the panel pockets formed by the intersection of the stiffeners. For additional information of these options, refer to the work by Mulani, Duggirala, and Kapania (ref. 17).

SECTION 3
PANEL DESIGN AND OPTIMIZATION

Initially, a 24-inch by 28-inch stiffened panel with six *T*-stiffeners was optimized with different options for stiffener placement. The stiffener endpoints were allowed to move on the horizontal edges only so that the stiffeners would align in the vertical direction or major compression direction (ref. 17). Figure 3 shows the boundary conditions and the applied loads. During the optimization using *EBF3PanelOpt*, the loads were applied through the stiffeners with the option “Stiffener Loads” along with “Nonuniform Thickness” option for panel pockets and “Symmetric Design” for stiffener placement. The optimization was carried out using the “Genetic Algorithm” with 34 particles and 1000 iterations using VisualDoc (ref. 20) commercial optimization software. Currently, the non-dominated sorting algorithm (NSGA-II) (ref. 21) supports real design variables in VisualDoc. Table 1 provides the optimization parameters for this algorithm used for the analysis. For the details regarding the definition of the parameters, see reference 20. Sizing design variables like panel pocket thickness, web and flange thickness, web heights, and flange widths are allowed to change during the optimization, apart from the shape variables of the curvilinear *T*-stiffeners. The objective of the optimization was to minimize the mass of the panel with the constraints on the buckling, crippling, and yielding.

Three different optimal designs were obtained, and it was found that the majority of stiffeners were straight. Hence, a fourth optimal design was obtained with six straight stiffeners equally

distributed on the panel using only the sizing design variables. So, *20* particles were used to simulate GA optimization for the final design.

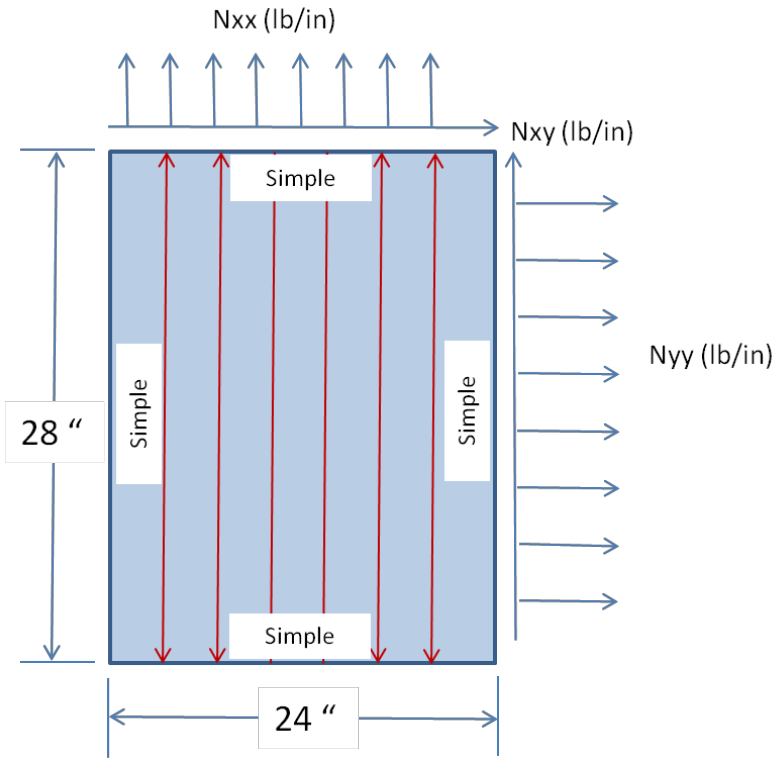

Figure 3. Skin panel geometry along with applied in-plane loads.

Table 1. VisualDoc optimization parameters for NSGA-II optimization (ref. 20).

Optimization Parameter	Value
Probability of Crossover	0.95
Probability of Mutation	0.10
Distribution Index for Crossover	10.00
Distribution Index for Mutation	15.00
Maximum number of iterations	1000

The panel was designed for a limit load of 85,440 lbs in compression against buckling, crippling, and yielding. Table 2 gives the material properties of the aluminum alloy used in the panel optimization. Table 3 gives the design variables along with their lower and upper bounds and with their optimal values for the final optimal panel. Figure 4 shows the thickness distribution, buckling mode shape, and von Mises stress distribution of the optimal design. Here, von Mises stress is normalized with respect to yield stress of the material, and the maximum stress is only 76 percent of the yield stress.

Table 2. Material properties for Al 2139 used for the panel optimization with *EBF3PanelOpt*.

Property	Value
Young's modulus, [Msi]	10.6
Poisson's ratio	0.33
Yield stress, [ksi]	61.9
Density, [lb/inch^3]	0.0975

Table 3. Design variable bounds and optimal values.

Design Variable	Lower Bound	Upper Bound	Optimized Design
Stiffener 1 Web Height, h_{w1}, [inch]	0.3937	1.9685	1.5328
Stiffener 2 Web Height, h_{w2}, [inch]	0.3937	1.9685	1.2763
Stiffener 3 Web Height, h_{w3}, [inch]	0.3937	1.9685	1.5892
Stiffener 1 Web Thickness, t_{w1}, [inch]	0.0394	0.3150	0.0606
Stiffener 2 Web Thickness, t_{w2}, [inch]	0.0394	0.3150	0.0942
Stiffener 3 Web Thickness, t_{w3}, [inch]	0.0394	0.3150	0.0653
Stiffener 1 Flange Width, w_{f1}, [inch]	0.3937	1.9685	0.3623
Stiffener 2 Flange Width, w_{f2}, [inch]	0.3937	1.9685	0.8218
Stiffener 3 Flange Width, w_{f3}, [inch]	0.3937	1.9685	0.4792
Stiffener 1 Flange Thickness, t_{f1}, [inch]	0.0394	0.3150	0.0803
Stiffener 2 Flange Thickness, t_{f2}, [inch]	0.0394	0.3150	0.0846
Stiffener 3 Flange Thickness, t_{f3}, [inch]	0.0394	0.3150	0.0532
Panel Pocket 1 Thickness, t_{p1}, [inch]	0.0394	0.1575	0.0888
Panel Pocket 2 Thickness, t_{p2}, [inch]	0.0394	0.1575	0.0919
Panel Pocket 3 Thickness, t_{p3}, [inch]	0.0394	0.1575	0.0845
Panel Pocket 4 Thickness, t_{p4}, [inch]	0.0394	0.1575	0.0942
Panel Pocket 5 Thickness, t_{p5}, [inch]	0.0394	0.1575	0.0829
Panel Pocket 6 Thickness, t_{p6}, [inch]	0.0394	0.1575	0.0907
Panel Pocket 7 Thickness, t_{p7}, [inch]	0.0394	0.1575	0.0872

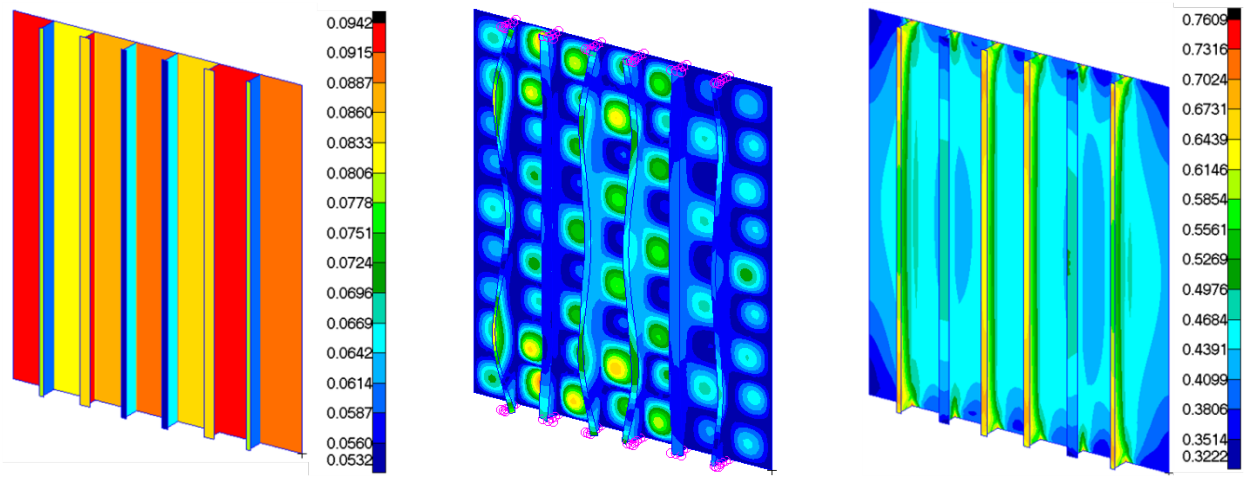

(a) Thickness distribution (in inches). **(b) Linear buckling mode shape.** **(c) Von Mises stress distribution.**

Figure 4. Optimal design responses for the applied in-plane compression.

The final optimized panel had six stiffeners with the dimensions of each stiffener, as well as each web segment between stiffeners, being optimized individually. Figure 5 shows the overall dimensions of the panel and the skin thickness in the individual pockets between stiffeners. Figures 6 and 7 show the dimensions of the *T*-stiffeners and the location of the stiffeners on the panel, respectively. The stiffener dimensions and locations are symmetric about the vertical centerline of the panel. However, the pocket thickness dimensions are not symmetric. The resultant panel had a weight of 8.3 lbs.

For comparative purposes, a baseline panel with six uniform *T*-stiffeners and a uniform web thickness was designed and optimized with conventional techniques, specifically a combination of HyperSizer and NASTRAN Solution 200. This conventional panel had a weight of 10.4 lbs. Thus, the panel that was designed and optimized with *EBF3PanelOpt* was able to achieve a weight reduction of 20 percent compared to the conventionally-optimized panel.

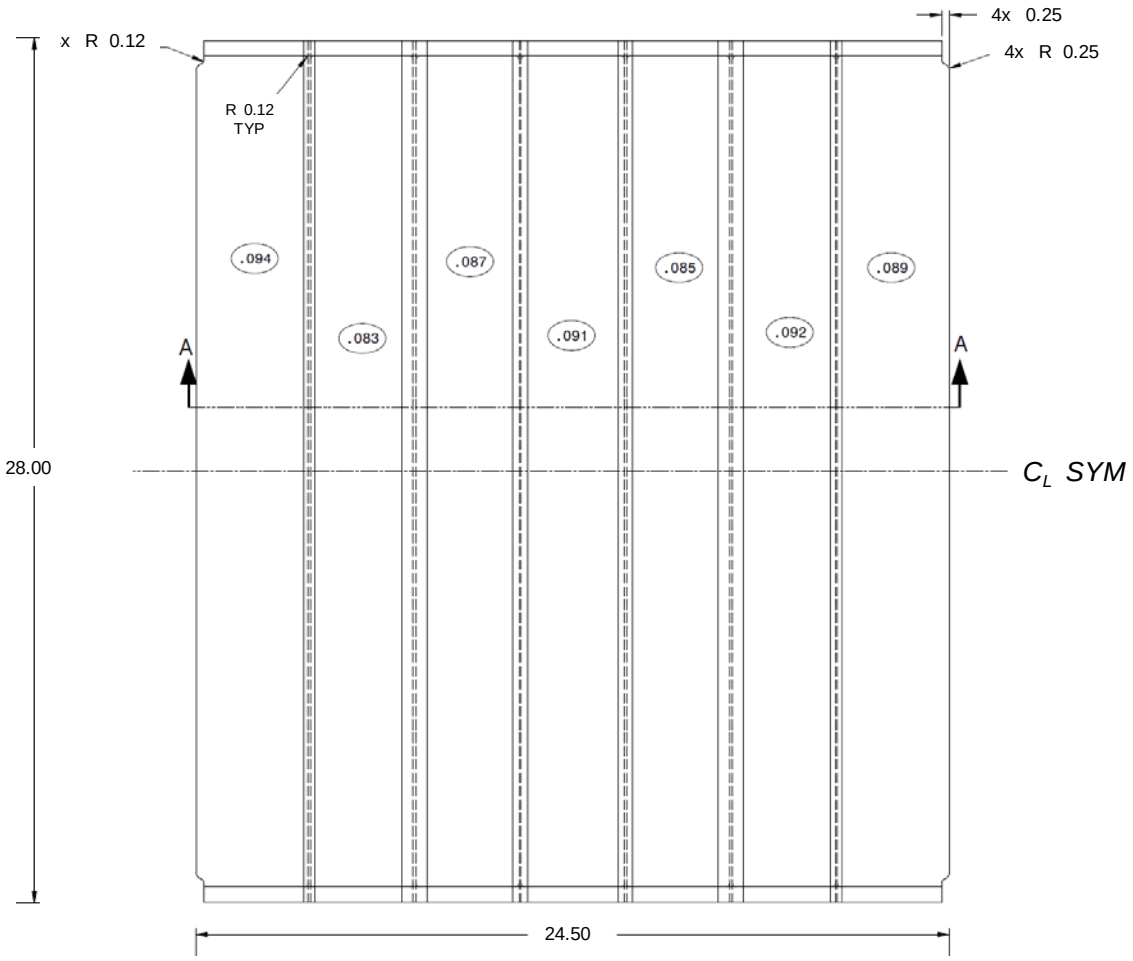

Figure 5. Overall dimensions of test panel and skin thickness for each pocket between stiffeners. (Dimensions are in inches.)

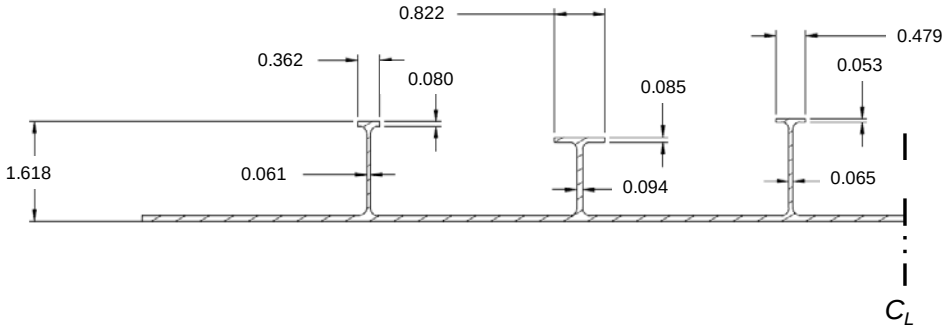

Figure 6. Dimensions of flanges and webs of *T*-stiffeners, viewing left half of Section A-A from Fig. 5. (Dimensions are in inches.)

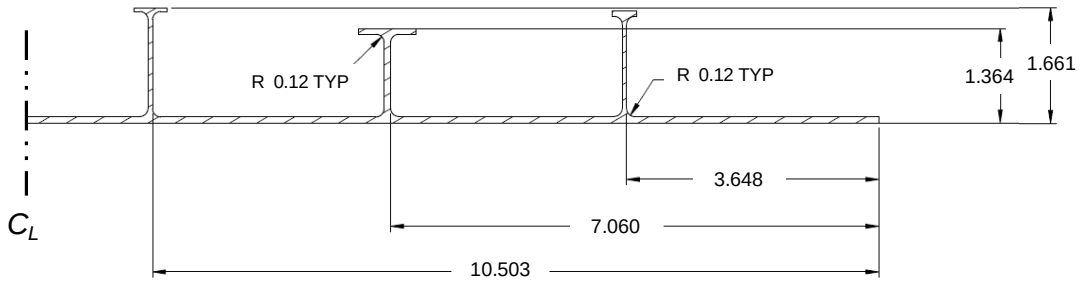

Figure 7. Location and height of *T*-stiffeners, viewing Section A-A from Fig. 5. (Dimensions are in inches.)

SECTION 4
PANEL MANUFACTURING

The final test panel was 28 inches tall by 24 inches wide and was machined from 2-inch thick 2139 aluminum plate using numerically controlled (NC) programming generated from a CAD file supplied by LM Aero. When the decision was made to apply only compression loading to this panel, the manufacturing effort was greatly simplified, compared to the previous combined loading test articles. The pad-ups and stiffener drop-off regions along the periphery of the test panel, as well as the bonded-on steel tabs, were no longer required to accommodate load introduction. The top and bottom ends of this panel were simply machined flat and parallel to ensure that an even distribution of loading was applied from the test machine platens. There were two deviations from the basic panel design cross section that were included in the test panel to simulate both vertical and lateral panel continuity during testing. The first was the minor pad-ups in the webs between the stiffeners at the top and bottom (loaded) ends of the panel. These were included to prevent a non-representative local web buckling at the loaded ends. The other deviation was to include a 0.25-inch extension of the web on each side of the panel to accommodate the anti-buckling guides, which would serve to simulate the next stiffener in an actual continuing panel. Post-machining inspection indicated that all stringent dimensional tolerance constraints specified on the manufacturing drawing were met. The panel was crated and shipped to NASA LaRC for final inspection, strain gage installation, and testing. Figure 8 shows a picture of the final machined panel.

Figure 8. Picture of the stiffened side of the Al–2139 test panel.

Once the panel was received at NASA LaRC, a surface profile of the test panel was generated laser scanning techniques. Figure 9 shows the deviation of the laser-scanned surface from that of the original CAD file of the panel. The center region of the panel had a surface profile similar to that of the original CAD file. However, one edge of the panel was bowed approximately 0.050 inch toward the smooth side. The other edge of the panel had a small twist such that the top corner bowed toward the smooth side and the bottom corner bowed toward the stiffener side by about 0.050 inch.

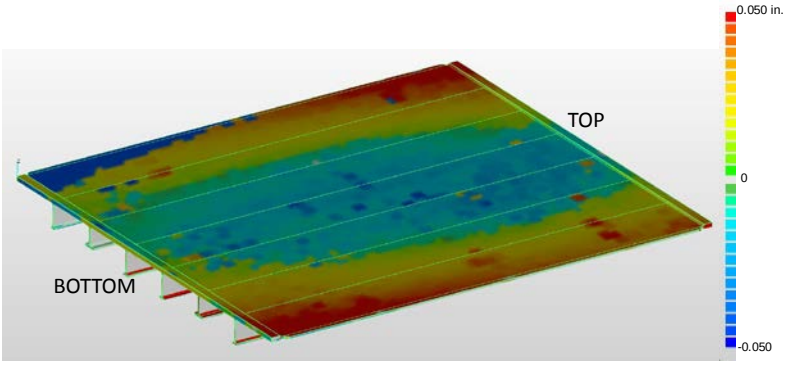

Figure 9. Laser scanned surface profile of *T*-stiffened panel compared to original CAD file.

SECTION 5
COMPRESSION TEST

A compression test was conducted on the *T*-stiffened panel at NASA LaRC with a 300,000-lb capacity hydraulic test machine. Linear variable displacement transducers (LVDTs) were attached to three corners of the upper compression platen to measure panel compression displacement.

A total of 36 strain gages were attached to the panel skin and stiffeners. Two of the gages were 0°/45°/90° rosettes and 34 of the gages were uniaxial gages aligned parallel to the compression load direction. Appendix A provides a description of the strain gage locations. The smooth (unstiffened) side of the panel was spray-painted with a speckled pattern to facilitate strain and displacement measurements with a Vic-3D (three dimensional) automated stereophotogrammetic technique. The panel was installed into the test machine with one LVDT located 0.75 inch above the center point of the panel on the stiffened side to measure out-of-plane displacement.

The data acquisition system was configured to scan and record all of the instrumentation at a rate of one scan per second. The load, displacements, and select strain gages were monitored on a real-time display during the test. The Vic-3D system was configured to obtain full-field stereophotogrammetic displacement and strain measurements on the smooth side of panel. In addition to the Vic-3D cameras, two video cameras were set up to record panel behavior during the test.

Anti-buckling guides were attached to the two edges of the panel to prevent premature buckling (see Fig. 10). The guides were tightened to the point where they were lightly clamping the panel but still allowed the panel to freely slide up and down within the guides. Teflon tape was applied to the edges of the panel to provide a low friction surface between the anti-buckling guides and the panel.

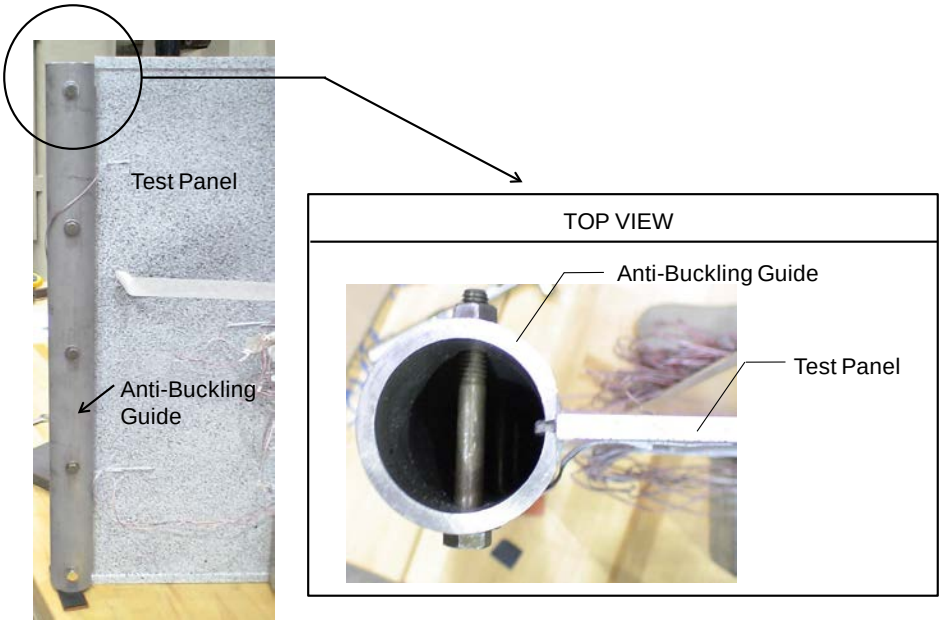

Figure 10. Anti-buckling guide.

Figure 11 shows the test system with the panel installed and ready for testing. Figure 12 shows the stiffened side and smooth side of the panel in the test system. A one-inch thick steel plate was situated between the bottom of the panel and the lower compression platen to prevent the panel from scarring the platen during testing. Similarly, a 0.03-inch thick sheet of titanium was positioned between the top of the panel and the upper compression platen. The panel was positioned in the test system such that the applied load was directly over the neutral axis of the panel cross section. The test system was configured to apply a compression load in stroke control at a displacement rate of 0.010 inch/minute. Preliminary tests were conducted up to a maximum compression load of 25,000 lbs to insure that all of the instrumentation was operational and that the panel was aligned and loading uniformly. Although a tight tolerance was put on the parallelism between the top and bottom edges of the panel, the preliminary tests indicated that 0.0015-inch thick foil shims were needed at the top of the panel in five locations. Figure 13 shows a picture of the shim locations. The data acquisition and Vic-3D systems were started, and the load application was initiated. Stiffener buckling events occurred at different load levels because the panel had three pairs of stiffeners with each pair having different dimensions and different buckling resistance levels. The first buckling event occurred at approximately 85,000 lbs. The load continued to increase to 133,500 lbs at which point the final pair of stiffeners buckled, and the load began to slowly decrease. The test was stopped at this point, and the panel was unloaded back to zero load. All six stiffeners buckled during the test, but the panel did not exhibit an abrupt catastrophic failure. Figure 14 shows a picture of the panel with buckled stiffeners following the compression test. The outermost stiffeners (A and D) buckled first, followed by the innermost stiffeners (B and C). Stiffeners E and F buckled last and do not show any significant nonlinearity in the figure because the test was stopped as soon as these stiffeners exhibited the onset of buckling.

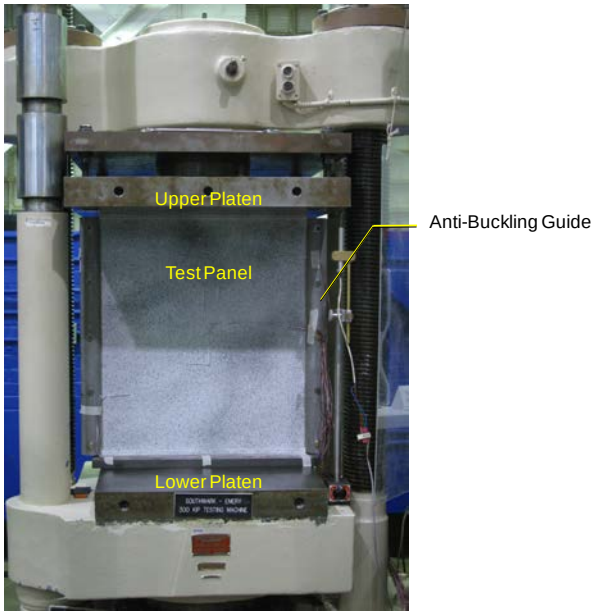

Figure 11. Compression test system with test panel installed.

(a) Stiffened side. **(b) Smooth side.**

Figure 12. Test panel in compression test system.

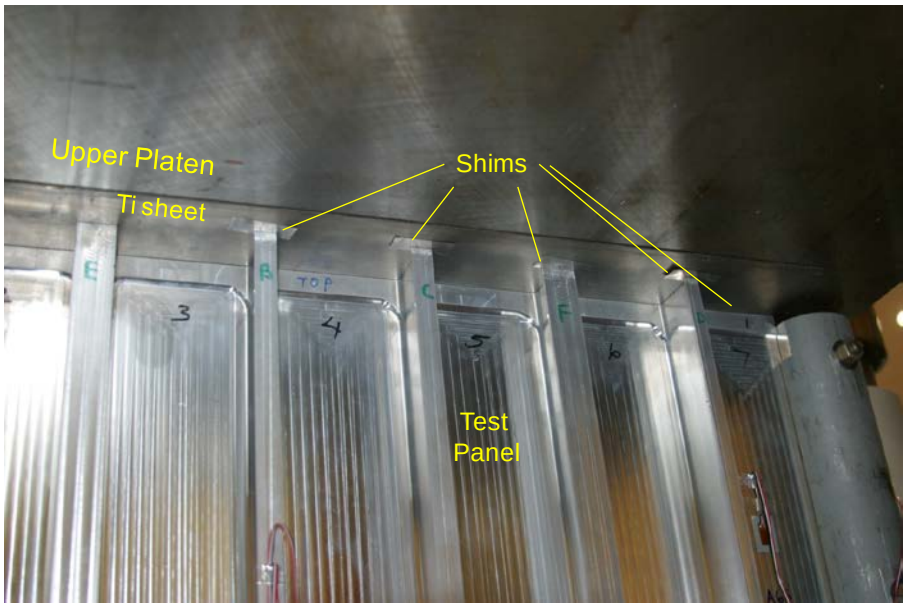

Figure 13. Shim locations at top of panel (four right-most stiffeners and right edge of panel).

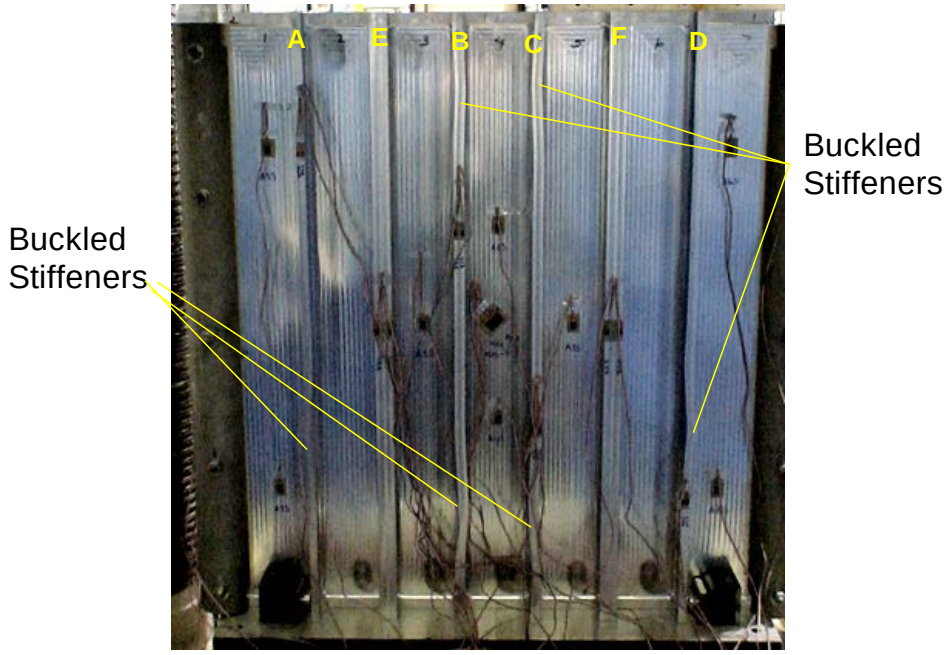

Figure 14. Post-test photograph showing locations where stiffeners buckled.

SECTION 6
COMPARISON OF EXPERIMENTAL AND ANALYTICAL RESULTS

The test results from strain gages and the Vic-3D image correlation system were compared with results from a nonlinear finite element model and the predicted linear response from the finite element model generated by the *EBF3PanelOpt* script. For all the results, the nondimensional load factor was used to indicate the load level during the proportionally loaded FEM and experiment. The load factor was defined as the ratio of applied load to linear buckling eigenvalue for the panel model. Appendix A describes the location of the strain gages. The responses from the complete set of strain gages were plotted against the load factor from the nonlinear finite element model and the experimental results in Appendix B.

Figure 15 shows the measured and predicted strain behavior for the *T*-stiffened panel skin on the upper right side (strain gage A6). The dashed curves represent test measurements from strain gages on the stiffened side (A6S) and on the smooth or "web" side (A6W). The solid curves are predictions. The vertical line represents the limit load generated by *EBF3PanelOpt*, which corresponds to a load factor of 1.0 or 85,440 lbs compression. Figure 16 shows the same information for the skin on the lower right side (strain gage A8). The data show that the panel buckled at the limit load as predicted.

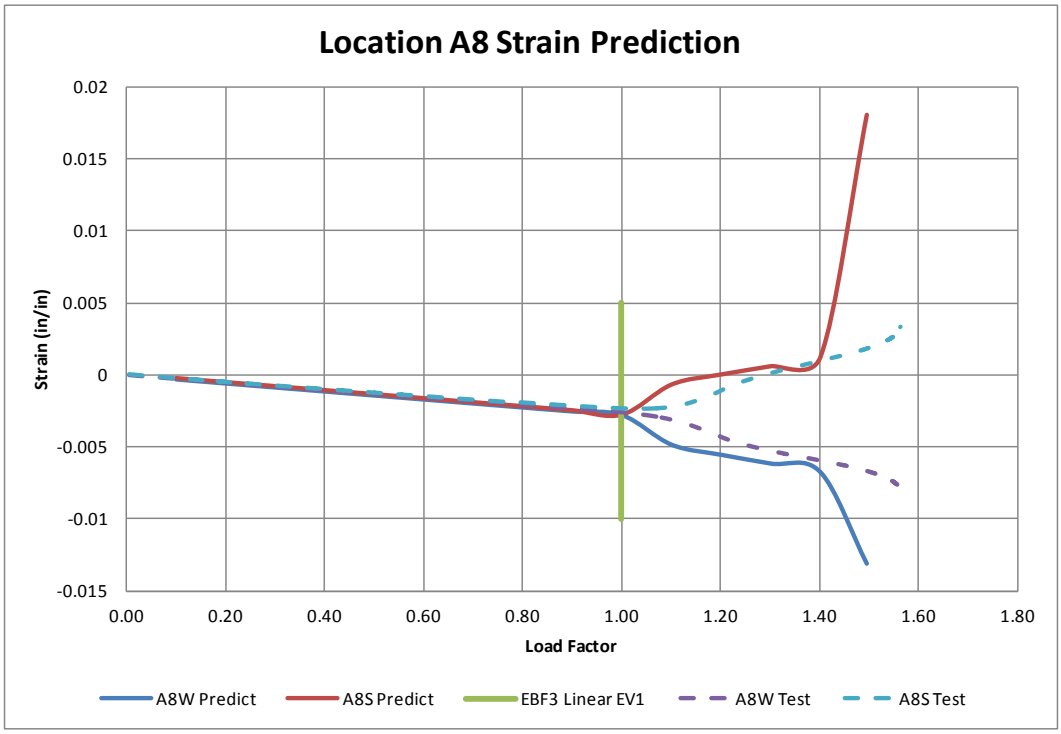

Figure 15. Measured and predicted strain behavior for the skin on the upper right side (strain gage A6 location).

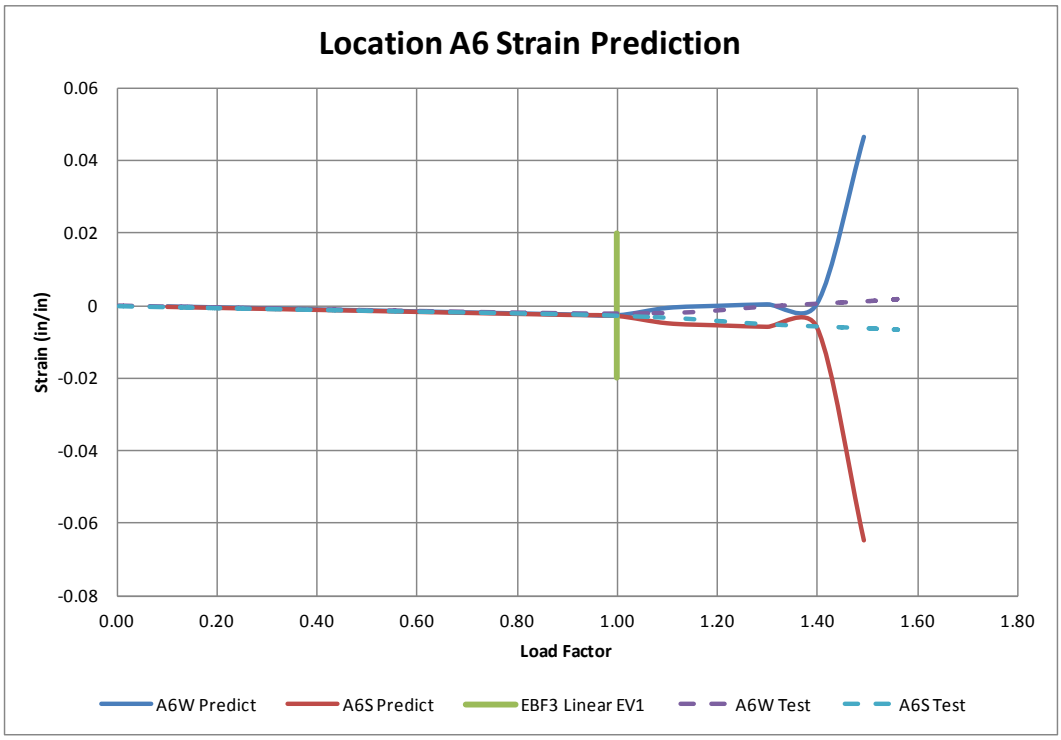

Figure 16. Measured and predicted strain behavior for the skin on the lower right side (strain gage A8 location).

The panel design was optimized such that the two outermost stiffeners (A and D) should also buckle at the limit load, followed by the two center stiffeners (B and C), and finally the middle stiffeners (E and F). Figure 17 shows the strain gage test data and predicted responses for the right-most stiffener (D). Strain gages S6A and S6B are located on the stiffener cap, and strain gage S6C is located on the smooth side of the panel directly behind that stiffener. The results indicate that this stiffener did buckle at the predicted limit load. Examination of all of the strain gage data for the stiffeners (not shown) showed that the stiffeners buckled in the sequence predicted, with the final set of stiffeners buckling at a load factor value of approximately 1.5.

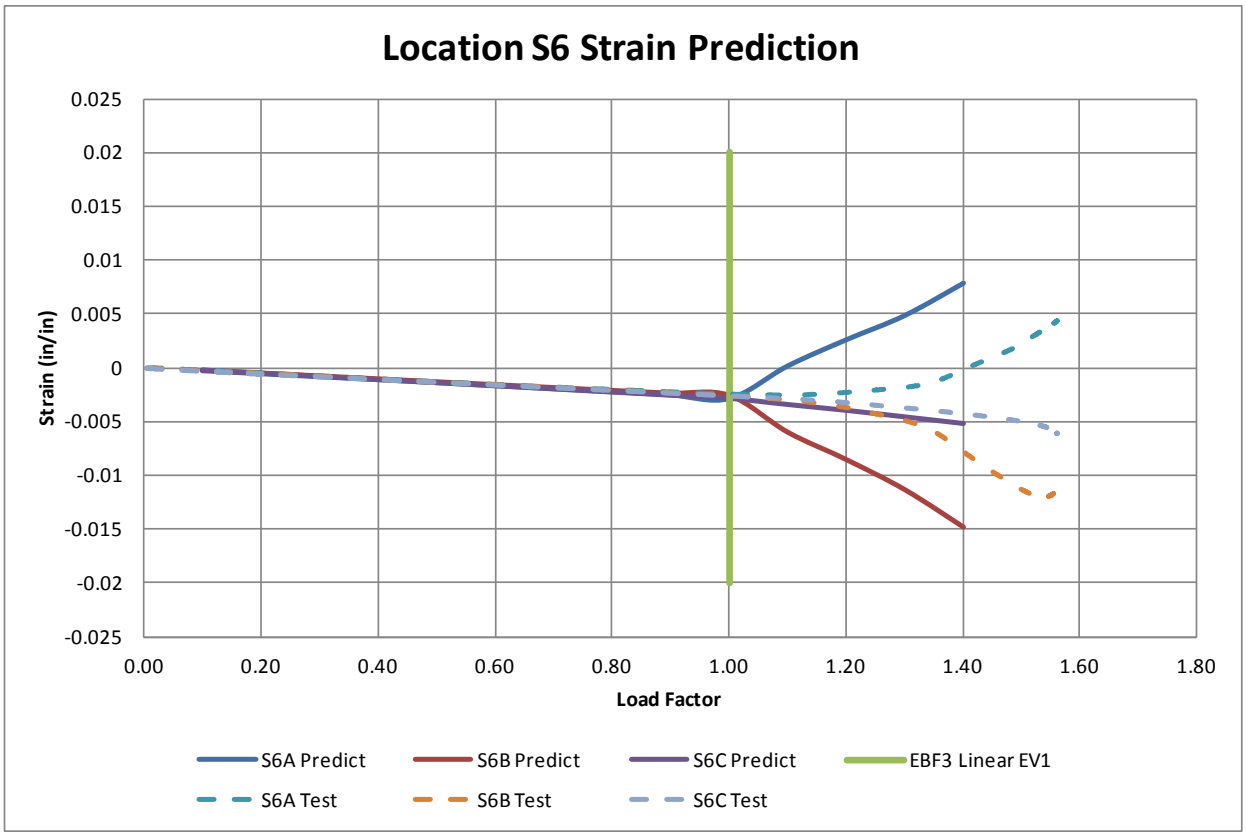

Figure 17. Measured and predicted strain behavior for the right-most stiffener (strain gage S6 location).

Comparison of predicted mode shapes matched very well with the test data recorded on the Vic-3D system. Figure 18 shows the out-of-plane displacement predicted and measured for the final buckled shape of the panel.

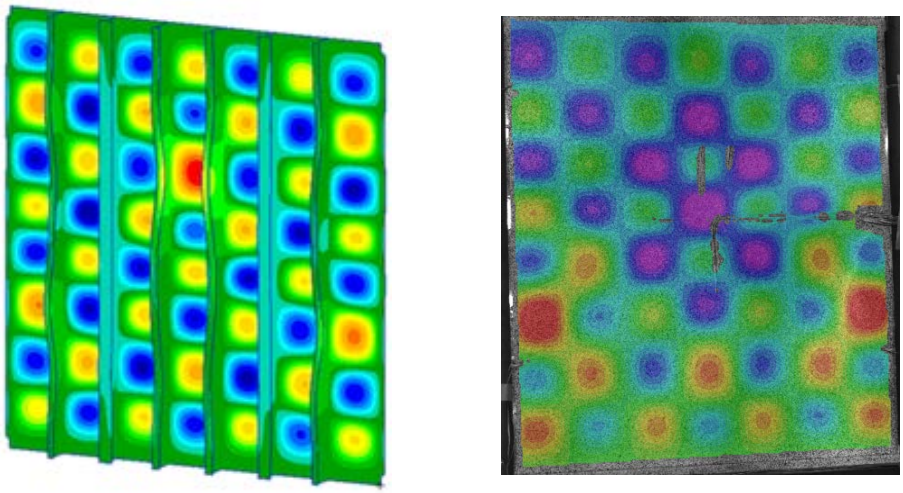

(a) Prediction. **(b) Vic-3D measurement.**

Figure 18. Out-of-plane displacement for panel at end of compression test.

As shown in Fig. 15–17, the predicted elastic strains were within just a few percent of the elastic strains from the test data. This result was typical for all of the strain gage locations (see Appendix B). The test data do show, however, that post buckling occurred at different load levels than predicted for some of the strain gage locations. This difference may be a reflection of post-buckling load redistribution within the panel not occurring as the analysis predicted. However, post-buckling behavior was reasonably predicted (both strain levels and modes) considering the highly nonlinear behavior of the panel. *EBF3PanelOpt* is a linear optimization code and does not rely on post-buckled behavior for optimization.

Analytical predictions indicated that catastrophic failure would occur rapidly in the load factor range of 1.40 to 1.49, with ultimate failure occurring at load factor of 1.49. The test data show catastrophic failure occurred at a load factor of 1.54. However, the test data did not show the predicted rapid failure because the test was conducted in displacement-control while the predictions were based on load-control conditions. Regardless, the ultimate failure occurred within 5 percent of the predicted load level.

In addition to good agreement between the prediction and the measurement for the strain behavior and buckling loads, the predicted buckling mode shapes matched very well with the test data recorded on the Vic-3D system. Figure 18 shows that the prediction and the Vic-3D measurement for out-of-plane displacement at the end of the test were very similar to each other.

SECTION 7
SUMMARY AND CONCLUSIONS

A *T*-stiffened panel was designed and optimized for minimum mass subjected to constraints on buckling load, yielding, and crippling, or to local stiffener failure a new analysis tool named *EBF3PanelOpt*. The panel was designed for a compression loading configuration that is a realistic load case for a typical aircraft skin-stiffened panel. The panel was integrally machined from 2139 aluminum alloy plate and was tested in compression. The panel was loaded beyond

buckling and strains, and out-of-plane displacements were extracted from 36 strain gages and one linear variable displacement transducer. A digital photogrammetic system was used to obtain full field displacements and strains on the smooth (unstiffened) side of the panel. The experimental data were compared with the strains and out-of-plane deflections from a high fidelity nonlinear finite element analysis. This design, optimization, and testing activity yielded the following conclusions:

- The panel optimized with *EBF3PanelOpt* with individually-optimized *T*-stiffeners had a weight that was 20 percent lower compared to a conventionally-optimized panel with uniform stiffeners.
- The panel is buckling-critical at limit load, as predicted by *EBF3PanelOpt*.
- Elastic strain predictions were within just a few percent of the measured values, further confirming the prediction that the panel was not strength-critical. This result implies the optimization routine correctly analyzed the critical failure mode and sizing (optimizing) accordingly.
- Post-buckled analysis (not required for *EBF3PanelOpt* validation) was reasonably representative of the panel behavior during testing, and catastrophic failure occurred within 5 percent of the predicted load level.

SECTION 8
REFERENCES

1. Collier, C., Yarrington, P., and West, B. V., "Composite, Grid-Stiffened Panel Design for Post Buckling Using Hypersizer," *43rd AIAA/ASME/ASCE/AHS/ASC Structures, Structural Dynamics, and Materials Conference*, No. AIAA–2002–1222, Denver, Colorado, 22–25 April 2002.

2. Anderson, M. S. and Stroud, W. J., "General Panel Sizing Computer Code and Its Application to Composite Structural Panels," *AIAA Journal*, Vol. 17, No. 8, 1979, pp. 892–897.

3. Bushnell, D., "Theoretical Basis of the PANDA Computer Program for Preliminary Design of Stiffened Panels Under Combined In-plane Loads," *Computers and Structures*, Vol. 27, No. 4, 1987, pp. 541–563.

4. Butler, R., Tyler, A. A., and Cao, W., "Optimum Design and Evaluation of Stiffened Panels with Practical Loading," *Computers and Structures*, Vol. 52, No. 6, 1994, pp. 1107–1118.

5. Stroud, W. J., Greene, W. H., and Anderson, M. S., "Buckling Loads of Stiffened Panels Subjected to Combined Longitudinal Compression and Shear: Results Obtained With PASCO, EAL and STAGS Computer Programs," Technical Paper 2215, NASA, 1984.

6. Renton, W. J., Olcott, D., Roeseler, W., Batzer, R., Baron, W., and Velicki, A., "Future of Flight Vehicle Structures (2000–2023)," *Journal of Aircraft*, Vol. 41, No. 5, 2004, pp. 986–997. doi:10.2514/1.4039.

7. Bendsoe, M. and Kikuchi, N., "Generating Optimal Topologies in Optimal Design Using a Homogenization Method," *Computer Methods in Applied Mechanics and Engineering*, Vol. 71, pp. 197–224, 1988.

8. Schramm, U. and Zhou, M., "Recent Developments in the Commercial Implementation of Topology Optimization," *IUTAM Symposium on Topological Design Optimization of Structures, Machines and Materials: Solid Mechanics and Its Applications*, Vol. 137, Part 6, 2006, pp. 239–248, doi: 10.1007/1–4020–4752–5_24.

9. Bendsoe, M. and Sigmund, O., *Topology Optimization: Theory, Methods, and Applications,* Springer-Verlag, Berlin, 2003.

10. Nicholas, E. D., "Developments in the Friction-Stir Welding of Metals," *ICAA–6: 6th International Conference on Aluminum Alloys*, 1998.

11. Taminger, K. M. B., Hafley, R. A., and Dicus, D. L., "Solid Freeform Fabrication: An Enabling Technology for Future Space Missions," *Keynote Lecture for 2002 International Conference on Metal Powder Deposition for Rapid Manufacturing Metal Powder Industries Federation,* San Antonio, TX, 8–10 April 2002, pp. 51–56.

12. Chan, K., Harter, J., Grandt, A. F., and Honeycutt, K., "Enhanced Crack Growth Methodology and Analyses for Unitized Structures," *Ninth Joint FAA/DoD/NASA Conference on Aging Aircraft*, Atlanta, GA, 6–9 March 2006.

13. Pettit, R. G., Wang, J. J., and Toh, C., "Validated Feasibility Study of Integrally Stiffened Metallic Fuselage Panels for Reducing Manufacturing Costs," NASA CR–2000–209342, The Boeing Company, Long Beach, CA.

14. Mulani, S. B., Joshi, P., Li, J., Kapania, R. K., and Shin, Y. S., "Optimal Design of Unitized Structures Using Response Surface Approaches," *Journal of Aircraft*, Vol. 47, No. 6, 2010, pp. 1898–1906.

15. Mulani, S. B., Slemp, W. C. H., and Kapania, R. K., "Development of a Framework for Design Optimization of Planar Panels Using Curvilinear Stiffeners," *Aeromat 2010 Conference and Exposition*, Bellevue, Washington, 20–24 June 2010.

16. Mulani, S. B., Slemp, W. C. H., and Kapania, R. K., "EBF3PanelOpt: A Curvilinearly Stiffened Panel Optimization Framework for Multiple Load Cases," *13th AIAA/ISSMO Multidisciplinary Analysis Optimization Conference*, Fort Worth, Texas, 13–15 September 2010, AIAA–2010–9238.

17. Mulani, S. B., Duggirala, V., and Kapania, R. K., "Curvilinearly *T*-Stiffened Panel Optimization Framework under Multiple Load Cases Using Parallel Processing," *53rd AIAA/ASME/ASCE/AHS/ASC Structures, Structural Dynamics, and Materials Conference*, Honolulu, Hawaii, 23–26 April 2012.

18. Kreisselmeier, G. and Steinhauser, R., "Systematic Control Design by Optimizing a Vector Performance Index," *Proceeding IFAC Symposium on Computer-Aided Design of Control Systems*, Zurich, Switzerland, 1979, pp. 113–117.

19. Niu, M. C. Y., ed. *Airframe Stress Analysis and Sizing*, 2nd Hong Cong: Conmilit Press, 1997.

20. VisualDOC 6.2, Design Optimization Software, Vanderplaats Research and Development, Colorado Springs, CO–80906.

21. Deb, K., Agrawal, S., Pratap, A., and Meyarivan, T., "Fast and Elitist Multiobjective Genetic Algorithm: NSGA-II", *IEEE Transactions on Evolutionary Computation*," Vol. 6, No. 2, 2002, pp. 182–197.

APPENDIX A
STRAIN GAGE LOCATIONS

A total of 36 strain gages were attached to the test panel. Two of the strain gages were type CEA–00–250UR–350 rosettes (0°/45°/90°) with the 90° direction oriented parallel to the compression load direction. The rosettes were attached to the skin in back-to-back fashion at the center point of the panel. Twenty-two of the gages were type CEA–00–250UW–350 uniaxial gages oriented parallel to the compression load direction. Sixteen of these gages were attached to the skin in back-to-back fashion in various locations remote from the stiffeners. In addition, six of these gages were attached to the skin on the smooth side of the panel directly behind each of the six stiffeners. The remaining 12 gages were type CEA–00–125UN–350 uniaxial gages oriented parallel to the compression load direction and were attached to the stiffener cap (two gages per stiffener).

Table A-1 shows an itemized list of the strain gages and their locations on the panel. Figure A-1 shows the strain gage locations on the skin on the stiffened side of the panel. The corresponding gages for the smooth side of the panel are directly behind those shown in the figure. The intersection of the vertical and horizontal centerlines is designated as the zero position point on the panel. The positive horizontal direction (x) on this drawing is pointing to the left on the stiffened side of the panel. The positive vertical direction (y) is pointing upward. The stiffener labels from left to right are A, E, B, C, F, and D. These labels are based on the stiffener section cut labels on the original panel drawing. Fig. A-2, A-3, and A-4 show the strain gage locations for each stiffener.

Table A-1. Location of strain gages on T-stiffened compression test panel.

gage ID	gage type	orient.	x (in)	y (in)	location
R1W1	rosette	0°	0.00	0.00	skin on smooth side of panel
R1W2	rosette	45°	0.00	0.00	skin on smooth side of panel
R1W3	rosette	90°	0.00	0.00	skin on smooth side of panel
R1S1	rosette	0°	0.00	0.00	skin on stiffened side of panel
R1S2	rosette	45°	0.00	0.00	skin on stiffened side of panel
R1S3	rosette	90°	0.00	0.00	skin on stiffened side of panel
A1W	axial	90°	3.43	0.00	skin on smooth side of panel
A1S	axial	90°	3.43	0.00	skin on stiffened side of panel
A2W	axial	90°	0.00	4.50	skin on smooth side of panel
A2S	axial	90°	0.00	4.50	skin on stiffened side of panel
A3W	axial	90°	–3.43	0.00	skin on smooth side of panel
A3S	axial	90°	–3.43	0.00	skin on stiffened side of panel
A4W	axial	90°	0.00	–4.50	skin on smooth side of panel
A4S	axial	90°	0.00	–4.50	skin on stiffened side of panel
A5W	axial	90°	10.30	8.00	skin on smooth side of panel
A5S	axial	90°	10.30	8.00	skin on stiffened side of panel
A6W	axial	90°	–10.30	8.00	skin on smooth side of panel
A6S	axial	90°	–10.30	8.00	skin on stiffened side of panel
A7W	axial	90°	10.30	–8.00	skin on smooth side of panel
A7S	axial	90°	10.30	–8.00	skin on stiffened side of panel
A8W	axial	90°	–10.30	–8.00	skin on smooth side of panel
A8S	axial	90°	–10.30	–8.00	skin on stiffened side of panel
S1A	axial	90°	stiffener A	4.50	cap on stiffener A
S1B	axial	90°	stiffener A	4.50	cap on stiffener A
S1C	axial	90°	1.71	4.50	skin on smooth side of panel behind stiffener A
S2A	axial	90°	stiffener E	–4.50	cap on stiffener E
S2B	axial	90°	stiffener E	–4.50	cap on stiffener E
S2C	axial	90°	–1.71	–4.50	skin on smooth side of panel behind stiffener E
S3A	axial	90°	stiffener B	0.00	cap on stiffener B
S3B	axial	90°	stiffener B	0.00	cap on stiffener B
S3C	axial	90°	5.14	0.00	skin on smooth side of panel behind stiffener B
S4A	axial	90°	stiffener C	0.00	cap on stiffener C
S4B	axial	90°	stiffener C	0.00	cap on stiffener C
S4C	axial	90°	1.71	0.00	skin on smooth side of panel behind stiffener C
S5A	axial	90°	stiffener F	8.00	cap on stiffener F
S5B	axial	90°	stiffener F	8.00	cap on stiffener F
S5C	axial	90°	1.71	8.00	skin on smooth side of panel behind stiffener F
S6A	axial	90°	stiffener D	–8.00	cap on stiffener D
S6B	axial	90°	stiffener D	–8.00	cap on stiffener D
S6C	axial	90°	1.71	–8.00	skin on smooth side of panel behind stiffener D

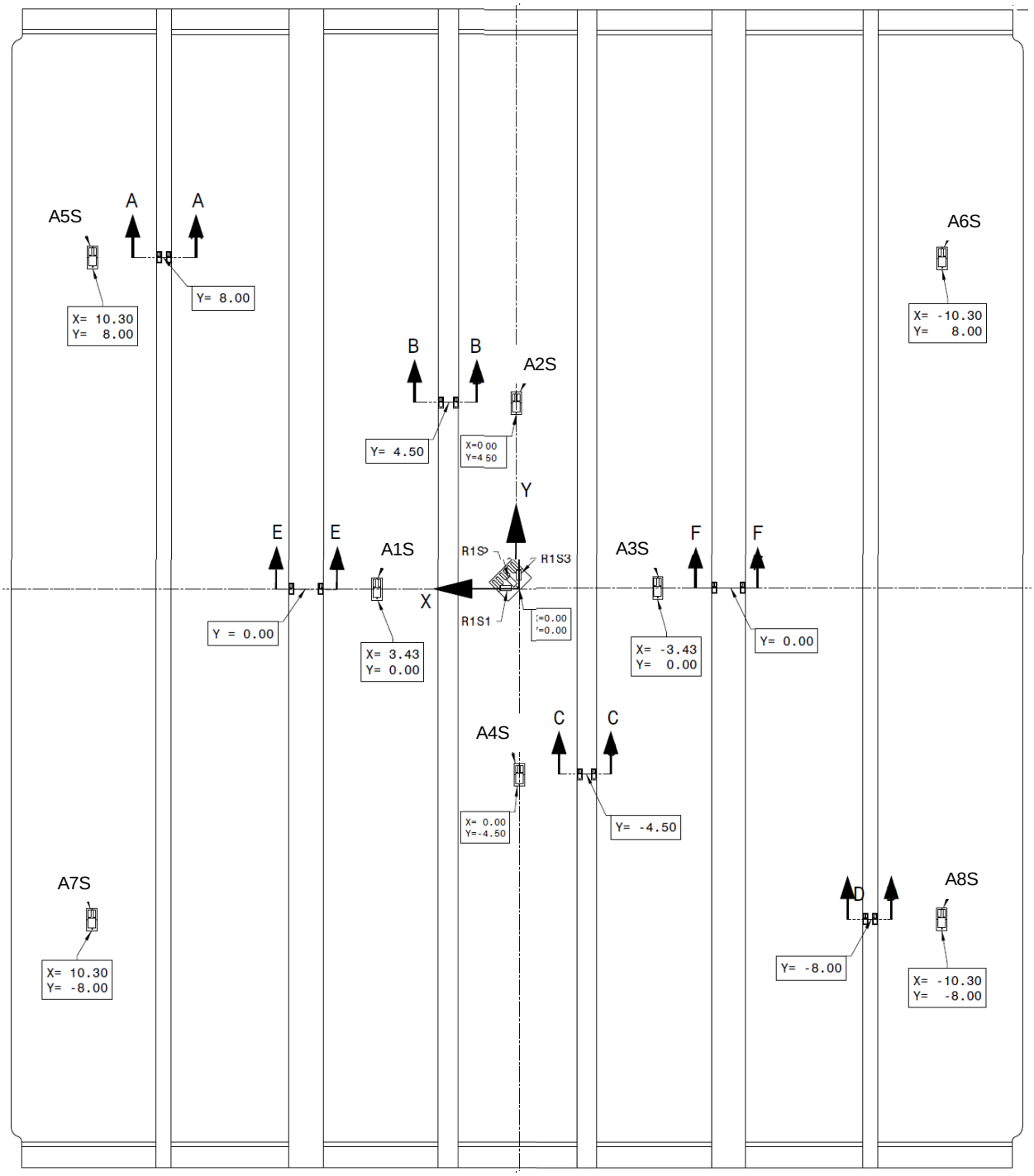

Figure A-1. Location of strain gages on the stiffened side of the test panel.

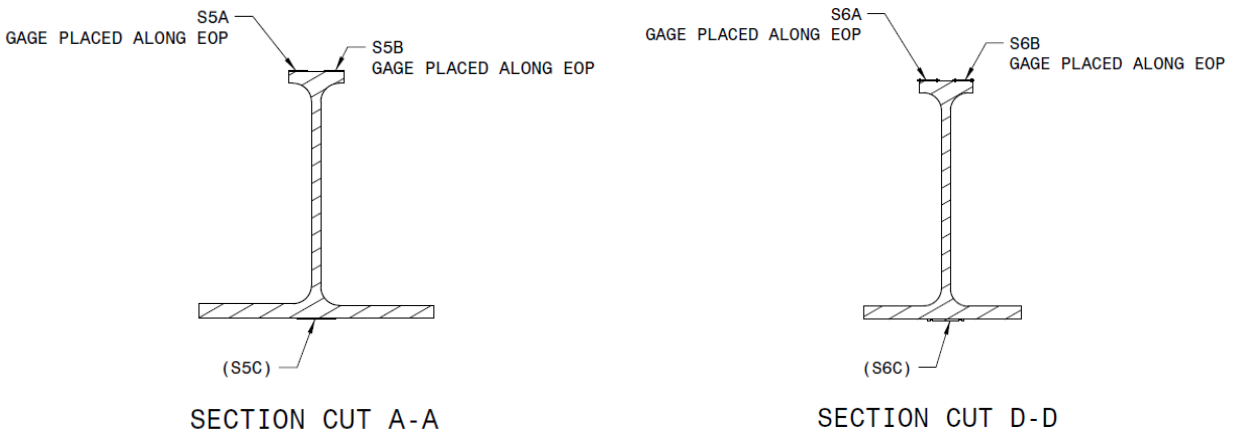

Figure A-2. Strain gage locations on stiffeners A and D.

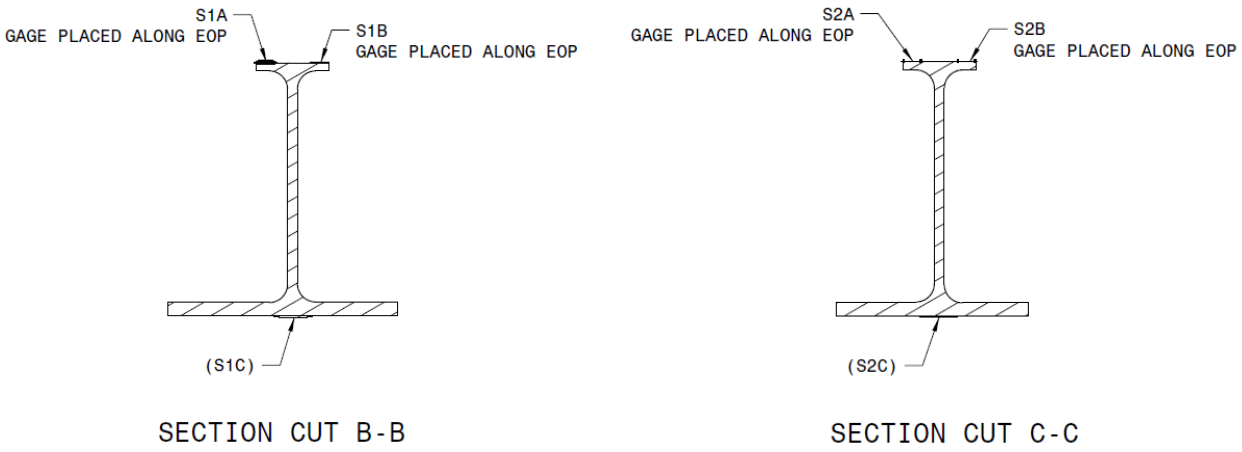

Figure A-3. Strain gage locations on stiffeners B and C.

Figure A-4. Strain gage locations on stiffeners E and F.

APPENDIX B
STRAIN GAGE PLOTS

The following figures show the data from each strain gage attached to the T-stiffened compression panel compared to the strain behavior prediction at that location. Also shown on each plot is the predicted buckling load factor as calculated from the linear eigenvalue generated from *EBF3PanelOpt*. A description of the strain gage locations is provided in Appendix A.

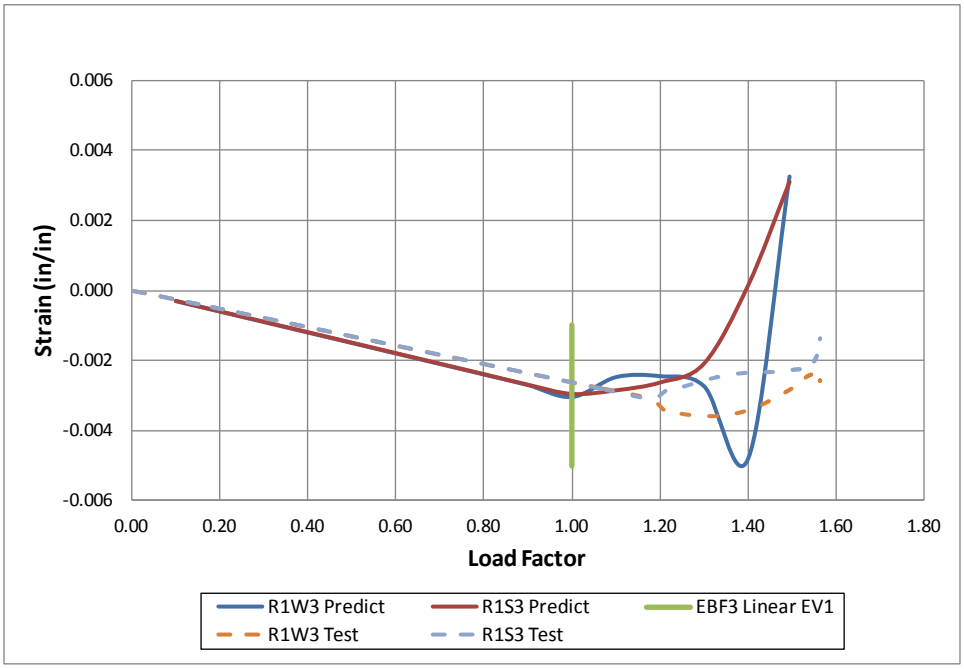

Figure B-1. Predicted and measured strain behavior at strain gage location R1. (Strain data are from the compression leg of the rosette gages.)

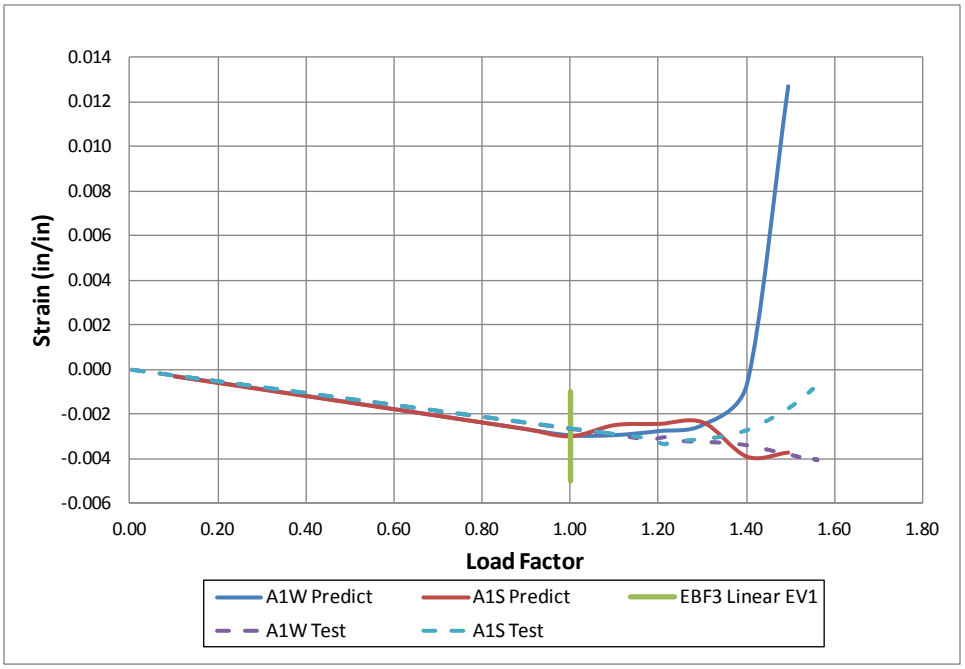

Figure B-2. Predicted and measured strain behavior at strain gage location A1.

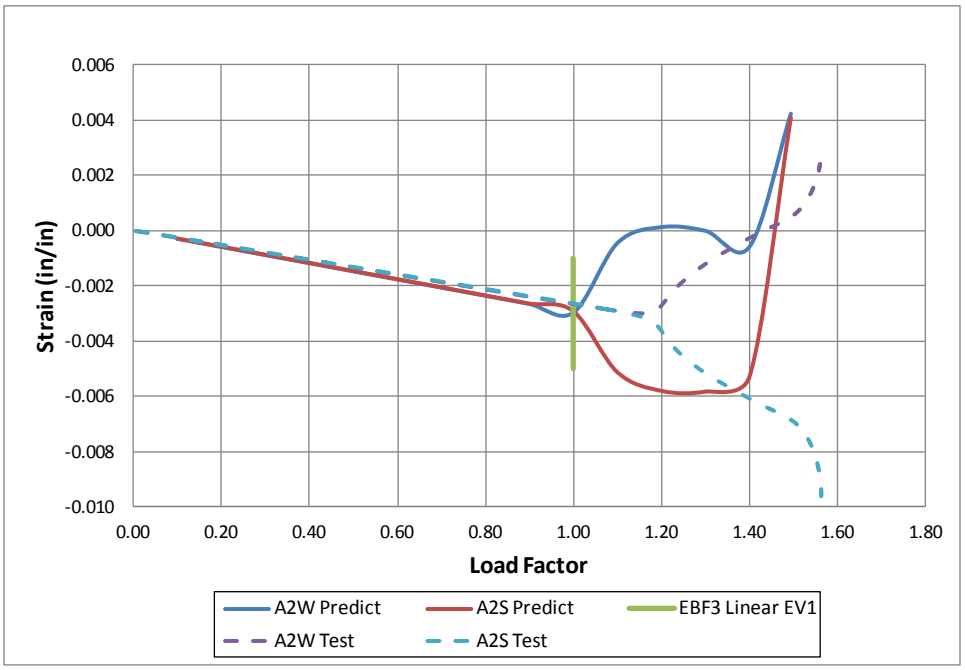

Figure B-3. Predicted and measured strain behavior at strain gage location A2.

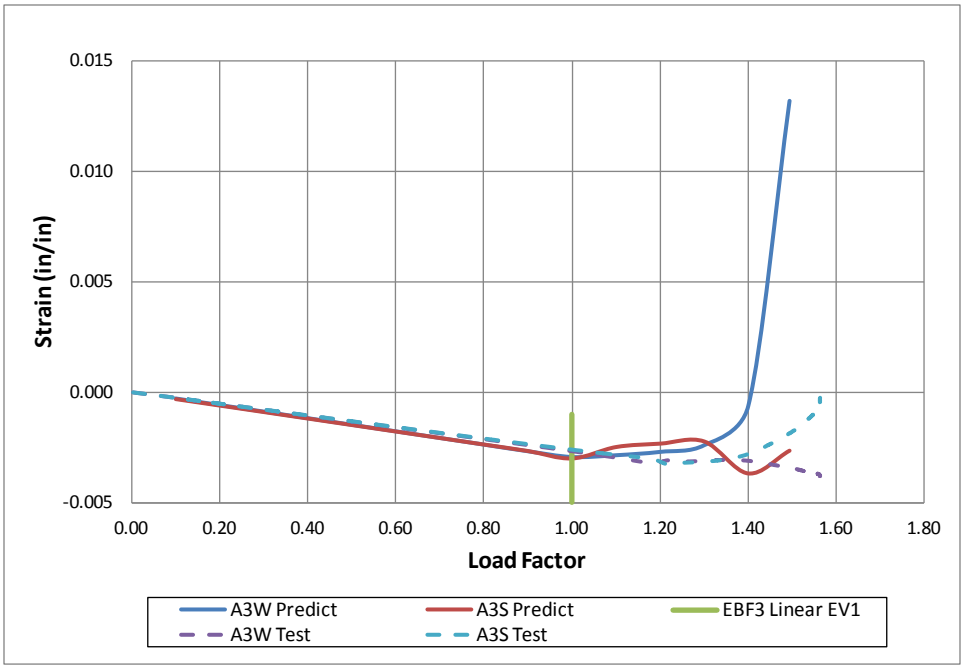

Figure B-4. Predicted and measured strain behavior at strain gage location A3.

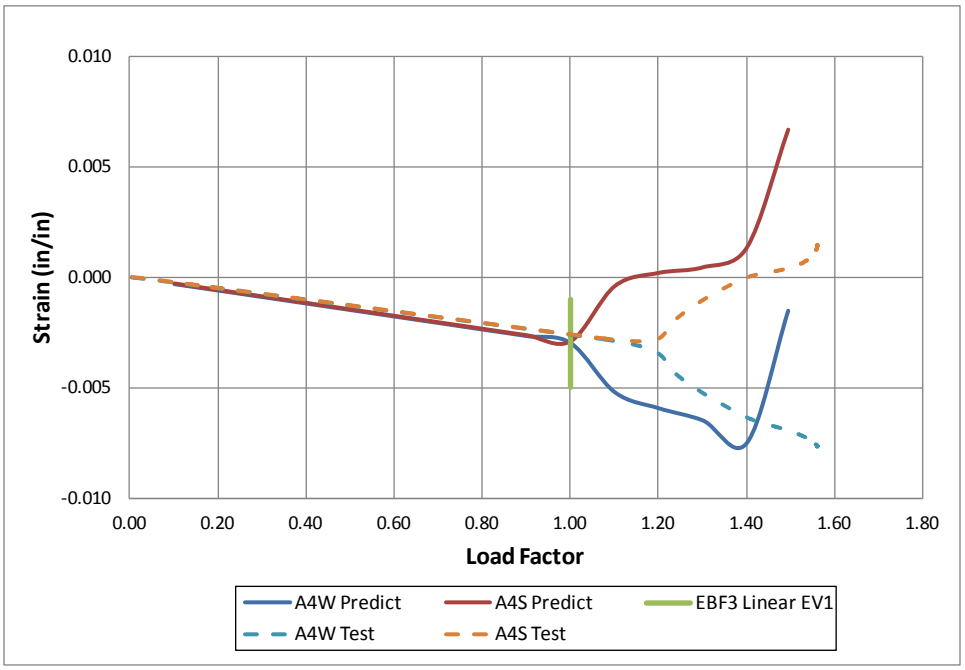

Figure B-5. Predicted and measured strain behavior at strain gage location A4.

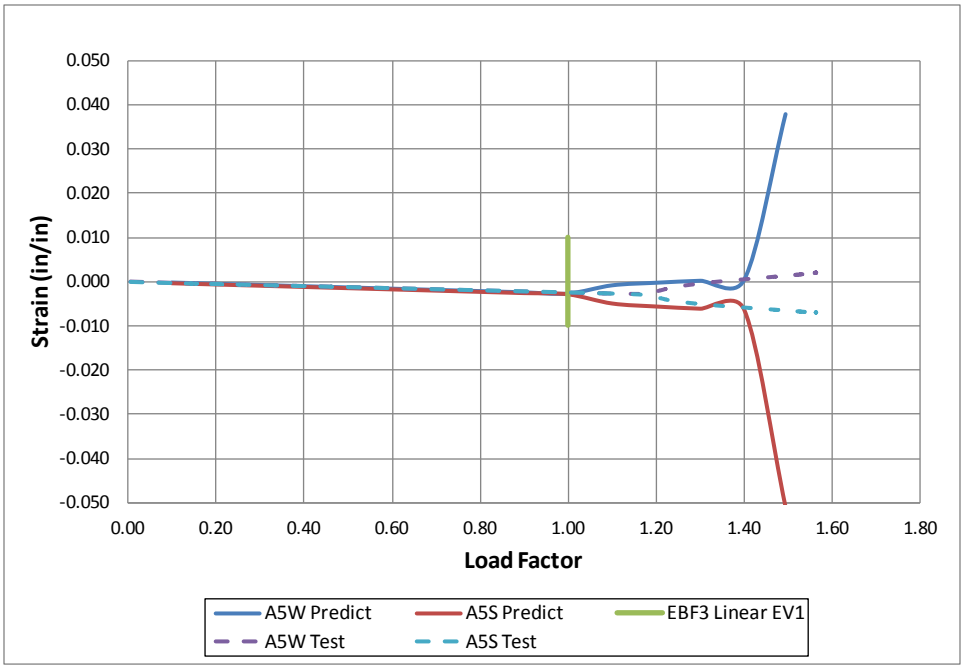

Figure B-6. Predicted and measured strain behavior at strain gage location A5.

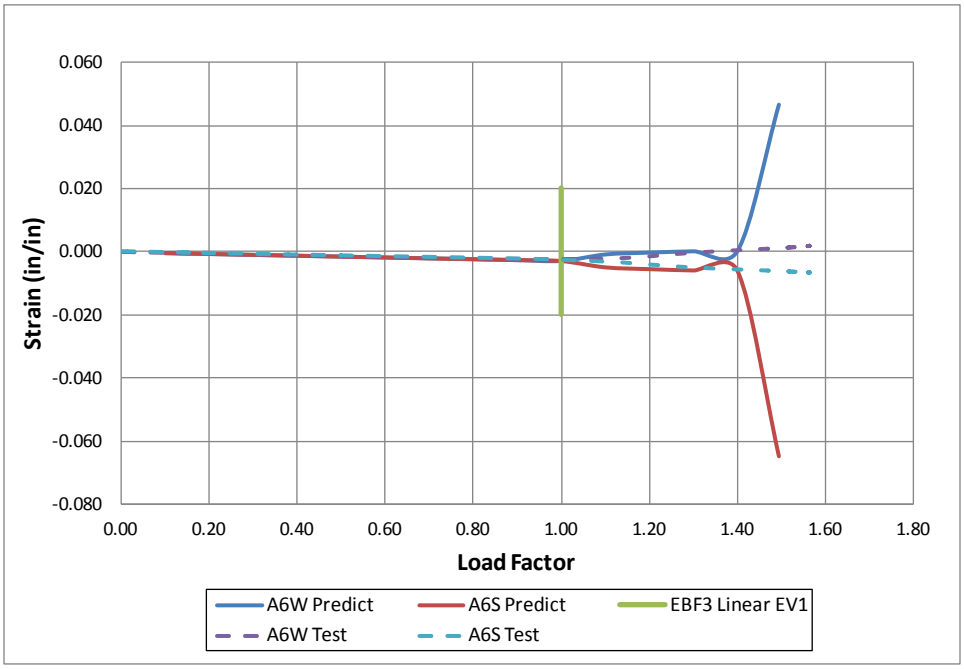

Figure B-7. Predicted and measured strain behavior at strain gage location A6.

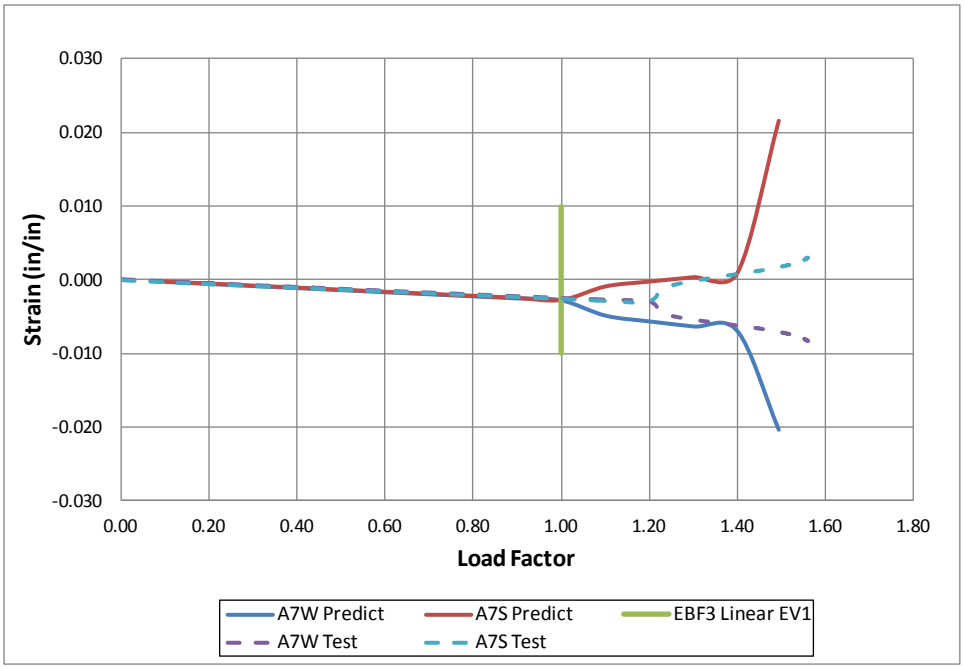

Figure B-8. Predicted and measured strain behavior at strain gage location A7.

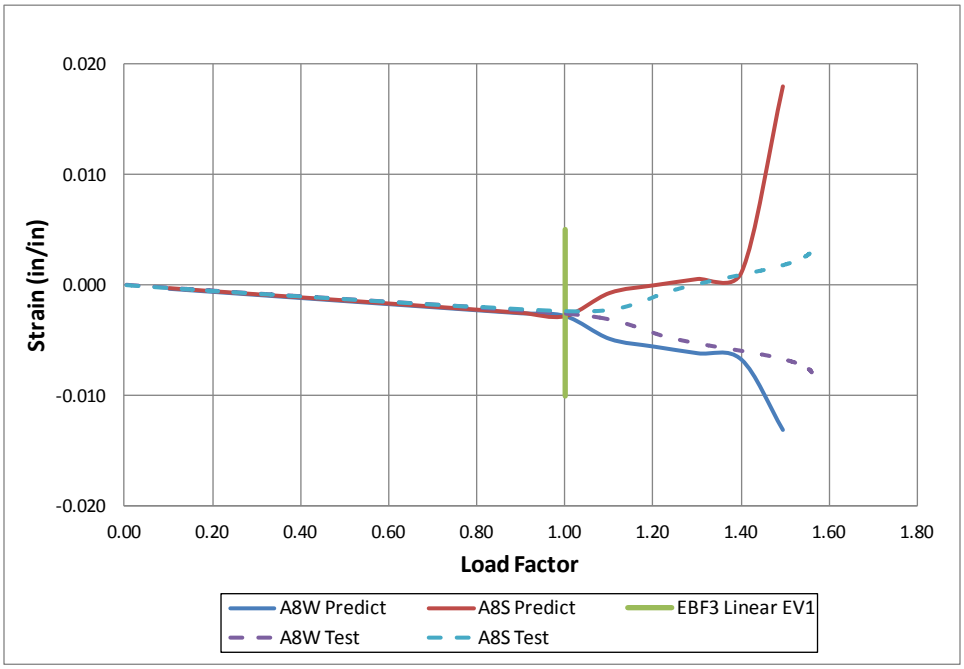

Figure B-9. Predicted and measured strain behavior at strain gage location A8.

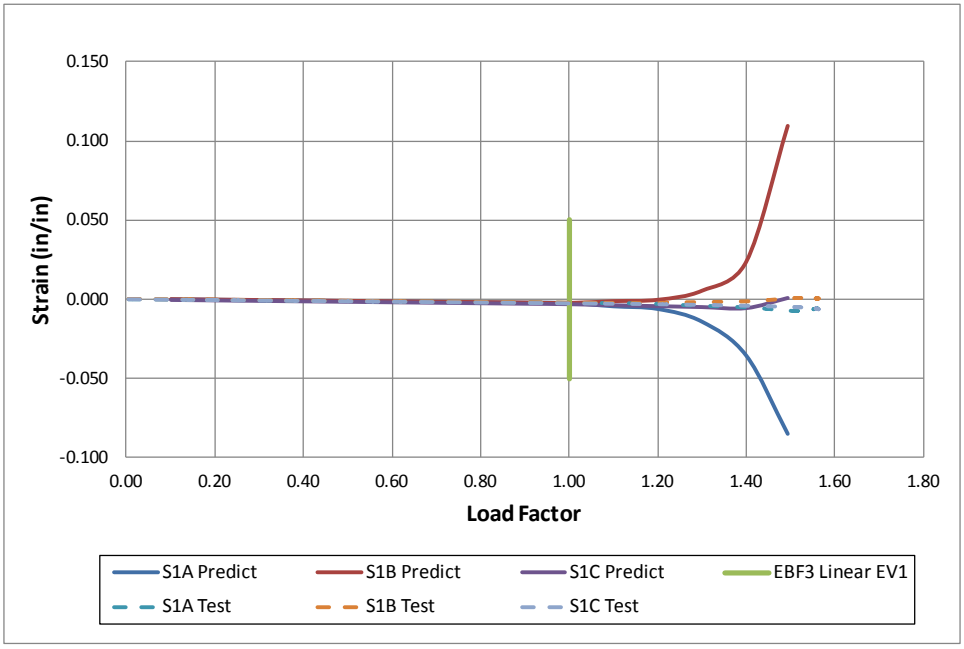

Figure B-10. Predicted and measured strain behavior at strain gage location S1.

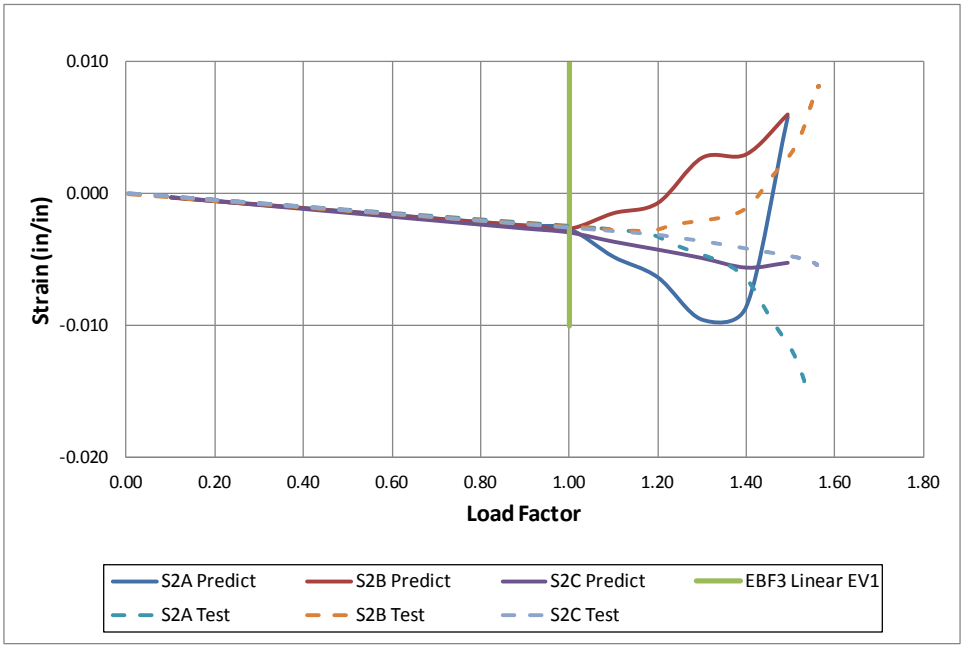

Figure B-11. Predicted and measured strain behavior at strain gage location S2.

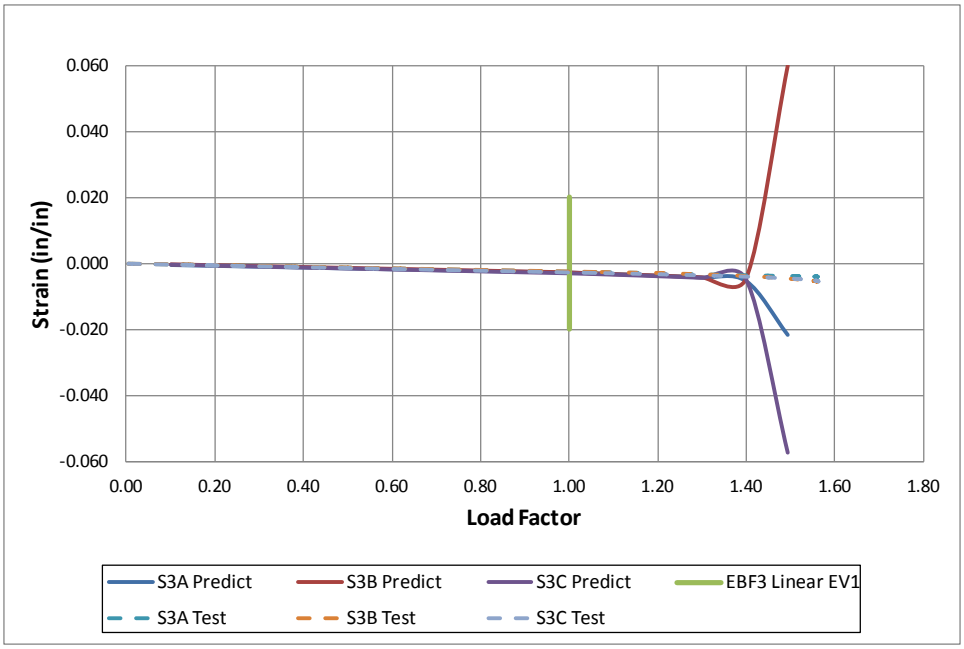

Figure B-12. Predicted and measured strain behavior at strain gage location S3.

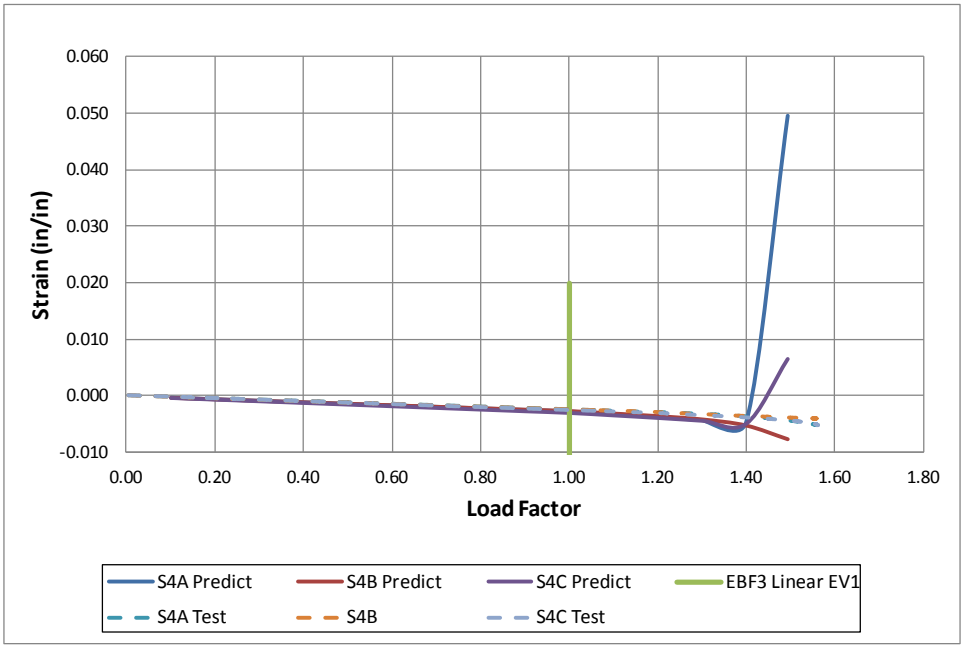

Figure B-13. Predicted and measured strain behavior at strain gage location S4.

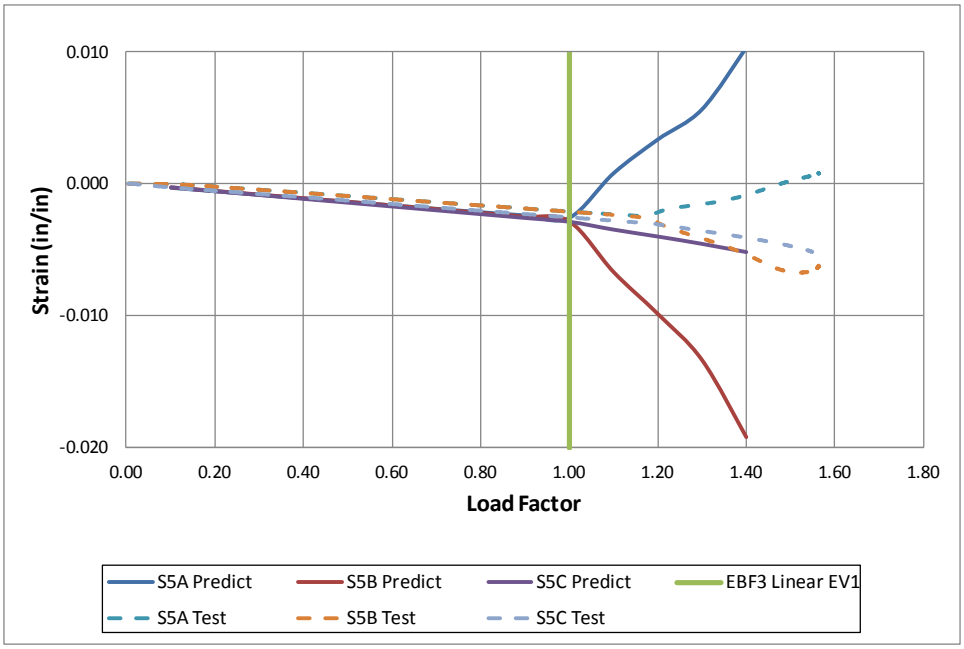

Figure B-14. Predicted and measured strain behavior at strain gage location S5.

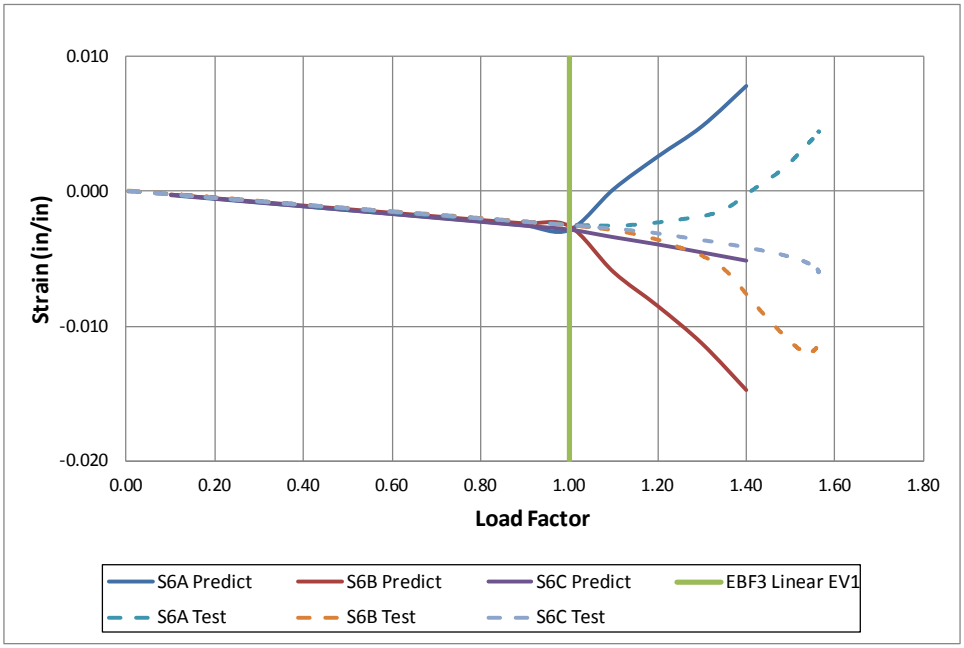

Figure B-15. Predicted and measured strain behavior at strain gage location S6.

REPORT DOCUMENTATION PAGE

Form Approved
OMB No. 0704-0188

1. REPORT DATE *(DD-MM-YYYY)*	2. REPORT TYPE	3. DATES COVERED *(From - To)*
01- 06 - 2012	Technical Publication	

4. TITLE AND SUBTITLE

Design, Optimization, and Evaluation of A1-2139 Compression Panel with Integral T-Stiffeners

5a. CONTRACT NUMBER

5b. GRANT NUMBER

5c. PROGRAM ELEMENT NUMBER

6. AUTHOR(S)

Mulani, Sameer B.; Havens, David; Norris, Ashley; Bird, R. Keith; Kapania, Rakesh K.; Olliffe, Robert

5d. PROJECT NUMBER

5e. TASK NUMBER

5f. WORK UNIT NUMBER

561581.02.08.07.43.01

7. PERFORMING ORGANIZATION NAME(S) AND ADDRESS(ES)

NASA Langley Research Center
Hampton, VA 23681-2199

8. PERFORMING ORGANIZATION REPORT NUMBER

L-20156

9. SPONSORING/MONITORING AGENCY NAME(S) AND ADDRESS(ES)

National Aeronautics and Space Administration
Washington, DC 20546-0001

10. SPONSOR/MONITOR'S ACRONYM(S)

NASA

11. SPONSOR/MONITOR'S REPORT NUMBER(S)

NASA/TP-2012-217584

12. DISTRIBUTION/AVAILABILITY STATEMENT

Unclassified - Unlimited
Subject Category 39
Availability: NASA CASI (443) 757-5802

13. SUPPLEMENTARY NOTES

14. ABSTRACT

A T-stiffened panel was designed and optimized for minimum mass subjected to constraints on buckling load, yielding, and crippling or local stiffener failure using a new analysis and design tool named EBF3PanelOpt. The panel was designed for a compression loading configuration, a realistic load case for a typical aircraft skin-stiffened panel. The panel was integrally machined from 2139 aluminum alloy plate and was tested in compression. The panel was loaded beyond buckling and strains and out-of-plane displacements were extracted from 36 strain gages and one linear variable displacement transducer. A digital photogrammetic system was used to obtain full field displacements and strains on the smooth (unstiffened) side of the panel. The experimental data were compared with the strains and out-of-plane deflections from a high-fidelity nonlinear finite element analysis.

15. SUBJECT TERMS

T-stiffeners; compression testing; finite element analysis; integral structures; structural optimization

16. SECURITY CLASSIFICATION OF:			17. LIMITATION OF ABSTRACT	18. NUMBER OF PAGES	19a. NAME OF RESPONSIBLE PERSON
a. REPORT	b. ABSTRACT	c. THIS PAGE			STI Help Desk (email: help@sti.nasa.gov)
					19b. TELEPHONE NUMBER *(Include area code)*
U	U	U	UU	44	(443) 757-5802